Single-Lipid Lamellar Hydrogels: from Gel Engineering to Soft Materials Design

Ghazi Ben Messaoud, Patrick Le Griel, Sylvain Prevost, Daniel Hermida-Merino, Wim Soetaert, Sophie Roelants, Christian Stevens, Niki Baccile

Single-Lipid Lamellar Hydrogels: from Gel Engineering to Soft Materials Design

Ghazi Ben Messaoud,[1,†] Patrick Le Griel,[1] Sylvain Prévost,[2] Daniel Hermida-Merino,[3] Wim Soetaert,[4] Sophie L. K. W. Roelants,[4,5] Christian V. Stevens,[6] Niki Baccile[1,*]

[1] Sorbonne Université, Centre National de la Recherche Scientifique, Laboratoire de Chimie de la Matière Condensée de Paris, LCMCP, F-75005 Paris, France

[2] Institut Laue-Langevin - 71 avenue des Martyrs CS 20156, 38042 Grenoble, France

[3] Netherlands Organisation for Scientific Research (NWO), DUBBLE@ESRF BP CS40220, 38043 Grenoble, France

[4] Ghent University, Centre for Industrial Biotechnology and Biocatalysis (InBio.be), Coupure Links 653, Ghent, Oost-Vlaanderen, BE 9000

[5] Bio Base Europe Pilot Plant, Rodenhuizekaai 1, Ghent, Oost-Vlaanderen, BE 9000

[6] SynBioC, Department of Green Chemistry and Technology, Ghent University, Coupure Links 653, 9000 Ghent, Belgium.

*Correspondence to: Dr. Niki Baccile, niki.baccile@sorbonne-universite.fr, Phone: 00 33 1 44 27 56 77

† Current address: DWI- Leibniz Institute for Interactive Materials, Forckenbeckstrasse 50, 52056, Aachen, Germany

Lipid lamellar hydrogels are rare soft fluids composed of a phospholipid lamellar phase instead of isotropic fibrillary networks. The mechanical properties of these thermodynamic materials are controlled by defects, induced by local accumulation of a

polymer or surfactant. In this work, we present a new class of kinetically-trapped, lipid lamellar hydrogels, composed of one single glycolipid, self-organizing into a biphasic lamellar fluid. Small angle x-ray and neutron scattering (SAXS, SANS), polarized light microscopy, rheology and rheo-SAXS show a gel with elastic modulus > 10^4 Pa possessing rheo-thinning properties with second-scale recovery, making it processable into soft 3D materials like beads or fibers, outclassing the properties of existing synthetic lamellar hydrogels. The properties and easy preparation methods open new perspectives in using biobased lamellar hydrogels in additive manufacturing, pharmacology or tissue engineering.

2D and 3D soft self-assembled materials, usually obtained from stimuli-responsive peptides, proteins and lipids,[1–4] attract a large interest in the field of nanotechnology, for the increasing number of high-tech applications[5] such as protective coating for cells,[6] regenerative medicine,[7] lab-on-a-membrane prototyping,[8] self-healing materials.[9] Lipids can self-assemble into a variety of soft structures,[10] possibly leading to isotropic (entangled fibers) or anisotropic (lamellar) structures, the latter being of particular interest.[11]

Lamellar hydrogels,[12] discovered in 1996 by Safinya and Davidson and composed of a phospholipid L_α phase stabilized by a polymer-grafted lipid, were the first example of an elastic 2D self-assembled material at small concentration (<10 wt%). Since then, lamellar hydrogels (LH) were obtained by polymer-stabilization,[13] or by combining a lamellar phase with a gelator.[14,15] The first polymer-free LH, based on surfactant mixtures or lipid/surfactants, are reported only in 2014.[16,17] Nonetheless, LH are rare compared to more common self-assembled fibrillary network, and their out-of-equilibrium manipulation is not known. If LH are complex elastic fluids generated by defects,[12] and of which the mechanical

properties are hard to control, their defectuous nature is also an opportunity in preparing new materials.[18]

We have recently shown that a pH-responsive glucolipid (**Figure 1**) below 1 wt% undergoes a reversible phase transition from a predominant micellar phase to flat interdigitated lipid layers (IL, **Figure 1**) from basic to neutral pH (transition pH ~7.8) at room temperature (RT).[19,20] The corresponding monounsaturated glucolipid is entirely derived from glucose and vegetable oil, fermented by the yeast *S. bombicola ΔugtB1*,[21] and lastly hydrogenated. The microorganism was specially engineered from the WT *S. bombicola*, known to produce the common sophorolipid biosurfactant. Deletion of the second glucosyltransferase (ugtb1) results in the direct production (as high as ~0.5 $gL^{-1}h^{-1}$) of glucolipids, up to then produced only by enzymatic conversion of acidic sophorolipids or by the microbial conversion of secondary alcohols glucosides.[22,23] The acidic glucolipid, simple in structure, combines a packing parameter >0.5 with a melting temperature (T_m) above RT, thus favouring the spontaneous formation of infinitely flat lamellae over vesicles.[20]

We show here that a phospholipid-free solution only containing glucolipid G-C18:0 (**Figure 1**) in the form of IL spontaneously forms a hydrogel in the neutral-acidic pH range above 1 wt%. The hydrogel is not fibrous, as expected from other microbial glycolipids,[24,25] but falls in the rare category of LH. The gels reach elastic moduli as high as 10 kPa, controllable by the ionic strength, in a pseudo two-phase lipid-water system, in the absence of any additive. pH controls the carboxylic/carboxylate ratio,[19,20] thus hiding an actual four-phase (neutral and charged glucolipid, water, salt) system, becoming the first single-molecule lamellar hydrogel. The hydrogel contains highly defectuous lamellar regions having shear-thinning properties with instantaneous (seconds) recovery of the elasticity, a property which we exploit to prepare millimeter-scale soft prototypes. Finally, the glycosylated nature of the

molecule defines a new class of lamellar glyco-hydrogel with potential interest in the biomedical field, cosmetics or food science.

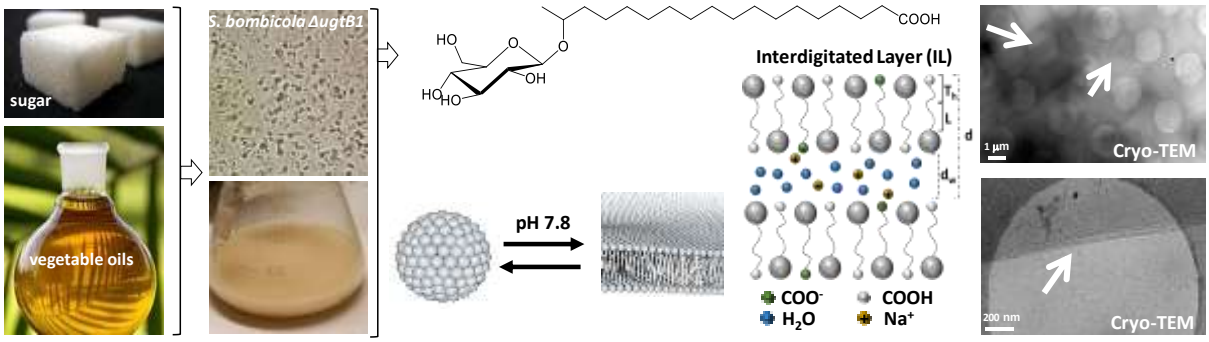

Figure 1 – Molecular structure of glucolipid G-C18:0 and its pH-dependent phase behavior at room temperature: a micelles-rich phase occurs at pH above 7.8 and a lamellar phase forms at pH below 7.8.[19,20] **G-C18:0 glucolipid is derived from the fermentation broth of *S. bombicola ΔugtB1* in the presence of glucose and vegetable oils. On the right-hand side, arrows superposed to the typical cryo-TEM images point at the typical infinite layered structure and stacking (pH ~6, $C_{G\text{-}C18:0}$= 1 wt%).**

Glucolipid G-C18:0 spontaneously forms lamellar hydrogels in water without additives

G-C18:0 is a microbial glycolipid characterized by a single glucose moiety covalently attached to stearic acid. A combination of SAXS and cryo-TEM data reported earlier[19,20] have shown the formation of a interdigitated layer (IL) exposing both the glucose and $COOH/COO^-$ moieties, where the $COOH/COO^-$ ratio depends on pH. **Figure 1** displays a scheme of the supposed structure of a G-C18:0 layer characterized by hydrophilic (T_h), hydrophobic (L) (total thickness, $2T_h+L= 3.6$ nm) and water layers (d_w).[19,20] Typical cryo-TEM images (and white arrows therein) recorded at pH ~6 (**Figure 1**) are presented to recall the infinitely wide structure of the G-C18:0 stacked layers.[19,20]

G-C18:0 hydrogels, which can be formed by its simple dispersion in water at room temperature at concentrations above about 1 wt%. The equilibrium pH is generally below 4.5, and under these conditions G-C18:0 is insoluble in water. Hydrogels can then be obtained by combining adjustment of pH in the range between 5 and 7.5 and using sonication (in a classical bath) during 20 to 30 min. These conditions generally provide a viscous solution (**Figure 2a1**), which turn into a gel when salt (here, NaCl) is added to concentrations above 20 mM. According to the amount of salt, hydrogels look homogeneous and do not recover immediately after vortexing (**Figure 2a2**), or they can display an opal-like appearance and fast recovery (**Figure 2a3**).

In order to perform comparable rheology experiments, all samples studied in **Figure 2** were annealed through vortexing, heating at 70°C, above the T_m (**Figure S 1**) and cooling in the rheometer. This treatment promotes a gel-to-sol transition, where the sol is characterized by a fluid homogeneous solution containing small (10-50 μm) spherulitic inclusions (**Figure S 2.e-f**). The typical sol-to-gel transition upon cooling is measured in **Figure 2g** over 2h, during which both moduli (G´´>G´) have a steep increase, then oscillating at 25°C until G´>G´´. Gels are heterogeneous multiscale structures characterized by: 1) large (100-500 μm)

oriented lamellar domains (**Figure 2d$_4$-d$_5$** and **Figure S 2.g-j**); 2) an aqueous matrix composed of interconnected lamellar domains below 5 μm in size (**Figure 2d$_1$**, **Video 1,2**); 3) embedded spherulitic objects composed of folded lamellar domains of thickness less than 500 nm (**Figure 2d$_1$**, **Figure 2d$_2$** and **Video 3**).

The typical frequency sweep (G´(ω) and G´´(ω), respectively represented by full and open symbols throughout this work) of (annealed) lamellar glyco-hydrogel prepared at pH 6.5 for three ionic strengths are shown in **Figure 2b**. The typical range of G´ (ω= 6.28 rad·s^{-1}) range between 10^2 Pa and 10^4 Pa when ionic strength ranges between ~50 mM and ~ 500 mM, measured at pH 6 and pH 6.5 (**Figure 2c**). The magnitude of G´ falls in the same order as observed for polymer-stabilized $L_{\alpha,g}$[26] and polymer-free lamellar hydrogels.[16] **Figure 2b** also shows that G´ > G´´over the entire frequency range, an established criterion distinguishing gels from viscous liquids.[27] The typical viscoelastic response of G-C18:0 follows a power-law behavior over four orders of angular frequency magnitude. Both moduli scale as $G' \sim G_0' \omega^{n'}$ and $G'' \sim G_0'' \omega^{n''}$, where G_0' and G_0'' are pre-factors at ω= 1 rad·s^{-1} and $n' \sim n'' \sim 0.23$ the exponents. The distinctive power-law rheology response, reported for other soft materials,[28] indicates a broad distribution of relaxation times,[29] modeled for critical gels[30] and in soft glassy rheology.[31] The latter in particular considers that viscoelasticity is controlled by disorder, metastability and local structural rearrangements between the mesoscopic elements.[32] Thermal motion alone is not sufficient to reach complete relaxation and the system has to cross energy barriers, larger than typical thermal energies,[32] and related to lamellar rearrangement in our case. G-C18:0 hydrogels satisfy all criteria of a soft (G´~ 0.1-10 kPa) glassy material: weak power law of G´, $G'' \alpha\ \omega^n$ and aging behavior. However, a direct relationship between microstructure and mechanical response remains challenging.[33]

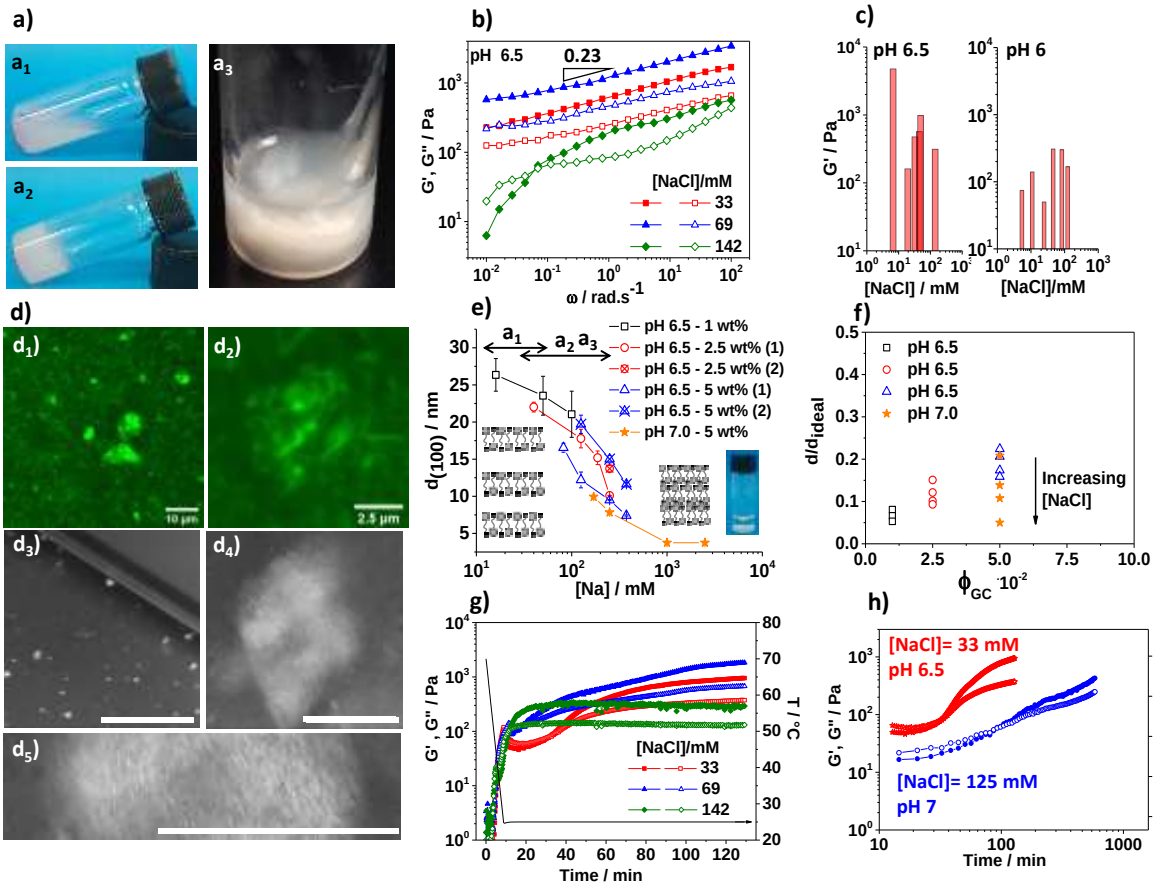

Figure 2 – a) Typical images of (a1) viscous and (a2, a3) gel solutions. Gel in a3 is denser and presents a stronger scattering than gel in a2. b) G´(ω) (full symbols) and G´´(ω) (open symbols) for $C_{G\text{-}C18:0}$= 2.5 wt% as a function of [NaCl] (pH= 6.5, γ= 0.05%). c) Typical absolute values of G´ at pH 6 and 6.5 as a function of [NaCl] (ω= 6.28 rad·s^{-1}, γ= 0.05%). d) Typical (d_1, d_2) confocal laser scanning microscopy (CLSM). Complementary CLSM videos (Video 1-3) are provided as Supporting Information. Polarized (d_3, d_4, d_5) light microscopy (PLM) (scale bar: 100 µm) and images of lamellar glyco-hydrogels; d_3 represents a typical viscous solution composed of $C_{G\text{-}C18:0}$= 1 wt%, pH 6.5, [Na$^+$]= 10 mM; d_1, d_2, d_4, d_5 represent a typical hydrogel composed of $C_{G\text{-}C18:0}$= 2.5 wt%, pH 6.5, [Na$^+$]= 150 mM. e) Evolution of the lamellar period $d_{(100)}$ as a function of ionic strength; the corresponding SAXS and SANS data are shown in Figure S 3. f) d/d_{ideal} ratio as a function of G-C18:0 volume fraction for different ionic strengths and pH values; d_{ideal}= δ/φ, being δ the membrane thickness (= 3.6 nm)[20] and φ the lipid volume fraction. g) Time evolution of G´ (full symbols) and G´´ (open symbols) at 25°C for various ionic strengths (cooling rate: 5°C/min, $C_{G\text{-}C18:0}$= 2.5 wt%, pH= 6.5, ω= 6.28 rad·s^{-1}, γ= 0.05%) after annealing (15 s vortex, loading, T= 70°C during 10 min, heating rate: 10°C/min). h) Comparison of the time evolution of G´ (full symbols) and G´´ (open symbols) after annealing at T= 70°C and cooling at 25°C for a gel ([NaCl]= 33 mM, pH 6.5) and a viscous

solution ([NaCl]= 125 mM, pH 7) (cooling rate: 5°C/min, $C_{G\text{-}C18:0}$= 2.5 wt%, ω= 6.28 rad·s^{-1}, γ= 0.05%). All rheology measurements are performed in a plate-plate geometry at constant normal force of 0 N (initial gap 0.5 mm).

SAXS (**Figure S 3a**) and SANS (**Figure S 3c-e**) experiments are recorded for samples at pH 7 and pH 6.5 and various NaCl concentrations. SAXS profiles measured at NaCl concentration below 250 mM bear a large oscillation above q= 1 nm^{-1} (**Figure S 3**a) and a -2 slope below q= 1 nm^{-1}; both features are typical of a lamellar form factor and they are analyzed in details (including fitting of SAXS data) for the same G-C18:0 sample elsewhere.[19,20] One should note that due to a different contrast, the oscillation in SANS profiles is not visible. Additionally, both SAXS and SANS profiles are characterized by a broad peak below 1 nm^{-1} and indicative or a lamellar period, $d_{(100)}$. Whichever the pH or technique of analysis, the peak is prominent for G-C18:0 concentrations above 2.5 wt% and NaCl content above about 100 mM, while below these values the peak is extremely broad and hard to observe. Kratky plots ($Iq^2(q)$, eliminating the q^2 dependence) in the insets of **Figure S 3c-e** are presented to help visualizing the peak for all samples.

Analysis of $d_{(100)}$ for all SAXS and SANS experiments shows that $d_{(100)}$ decreases with increasing ionic strength (**Figure 2e**), which proves that electrostatic repulsion controls the lamellar stacking.[34] The lamellar spacing for low concentrations and low ionic strength is ~20 nm, where larger spacing characterizes viscous fluids (**Figure 2a1**) and smaller spacings (< 15 ~nm) are generally associated to gels (**Figure 2a2,a3**). In the excess of salt (1 M), a powder, characterized of condensed lamellae, precipitates, as also shown by diffraction peaks becoming sharper, more intense, and shifting above 1 nm^{-1} (**Figure S 3a).**

The expected period for a lamellar phase is $d_{ideal}=\delta/\varphi$, being δ the membrane thickness (here assumed to be $2T_h+L=3.6$ nm)[20] and φ the lipid volume fraction. The glyco-hydrogels do not follow ideality (**Figure 2f**, $d/d_{ideal}<1$) below 10 wt% at any pH and ionic strengths,

suggesting that a second phase applies an additional osmotic pressure on the lamellae,[35] confirmed in this system by light microscopy discussed below.

The elastic properties of lamellar hydrogels depend on structural defects in the lamellar phase. Gel formation in polyethyleneglycol(PEG)-stabilized L_α phase depends on the PEG volume fraction, which, segregating into curved membrane regions, become a nucleation site of the defects.[12,26] Recently, Niu et al.[16] have supposed the origin of the elastic properties in polymer-free LH to depend on the edge accumulation of negatively-charged SDS surfactant. Polarized light microscopy (PLM) was used to identify structural defects, like sheet-like texture or spherulitic inclusions, in LH.[12,36] Typical PLM and CLSM images acquired on both viscous (**Figure 2d$_3$**, **Figure S 2.a-f**) and gels (**Figure 2 d$_1$,d$_2$,d$_4$,d$_5$**, **Figure S 2.g-h**) samples show a biphasic medium (explaining the non-ideal lamellar swelling) respectively containing small (1-50 μm) and large (100-500 μm) birefringent domains. Polarized and confocal microscopy confirm the widely defectuous nature of the gel (**Figure 2 d$_1$,d$_2$,d$_5$**; **Video 1,2**), recalling both the typical sheet-like/whispy texture (Figure 17G in Ref. 36) and spherulitic inclusions of LH. The latter are widely present in the gel and they are themselves composed of entangled lamellar domains (**Figure 2 d$_1$, d$_2$; Video 3**). A closer look to all data in our possession excludes a monophasic defectuous lamellar phase,[12,26] but rather a complex multiscale material composed of large (hundreds of microns) interconnected defectuous lamellar domains embedded in an aqueous environment containing smaller lamellar domains and lamellar spherulitic inclusions.

Time stability of the hydrogels over 24 h shows that weak gels (10^2 Pa) measured after 2 h from annealing (blue symbols in **Figure 2h**) evolve towards stronger gels (10^3 Pa) after 24 h, indicating that the evolution of the mechanical properties can occur on long time-scales. Quantitative observations up to 48 h (**Figure S 4**), and qualitatively over two weeks, show that initially viscous solutions systematically turn into gels, which eventually tend to scatter

light (whitening), to show syneresis and loose their mechanical properties after several days. The continuous evolution of the aspect and mechanical properties show that none of the lamellar glyco-hydrogels reach thermodynamic equilibrium, which makes it impossible to draw a consistent quantitative overview correlating mechanical properties and physico-chemical parameters. For this reason, most of the experiments presented in **Figure 2** are performed after an arbitrary lag time of two hours, at which the estimated concentration above which gelation is possible (here measured at pH = 6.7, ionic force 163 mM, **Figure S 5**) is in the order of 1 wt%.

pH and salt are known to strongly affect charged lamellar systems but the impact of salt on the mechanical properties of lamellar glyco-hydrogels is particularly astonishing and never reported for lamellar gels. pH plays on the ionization degree of G-C18:0 and, as a consequence, on the charge density of the interdigitated layers (IL). We have noticed that at low ionic strength (<~100 mM), pH plays a marginal role on the mechanical properties. At higher ionic strength, where charge screening can cause precipitation (d_w<1 nm), increasing pH promotes redispersion of the IL, most likely due to the introduction of negative charges in the membrane, allowing d_w to increase again. . At constant pH, increasing the ionic strength promotes shrinking of d_w in the 15 nm range and gel formation.

Transmission of the constraints in lamellar systems are promoted by defects in the flat IL, which can only occur if the line tension becomes locally small, promoting IL bending. This effect was achieved by PEG in LH, and we believe that salt has a similar role in the present lamellar glyco-hydrogels with negative charge density (pH>~5). It was shown before that charge and salt decrease the bending modulus and total bending energy of lipid IL.[37] The T_m of G-C18:0 is at 37°C, close to RT (**Figure S 1**), consequently, when the electrostatic repulsion is partially screened and its contribution to the bending modulus[38] is reduced, the IL is free to fluctuate and possibly bend, the curvature being stabilized by the negative charges.

This picture is also consistent with the idea that the glyco-hydrogel is a kinetically-trapped, out-of-equilibrium, phase. Addition of salt has an immediate impact on defect formation, reducing the percolation of water. Given the high viscosity, restructuring of the membrane becomes a long process and at constant pH and ionic strength, ion adsorption can occur with time, a phenomenon which was shown to be fast (hour) for divalent but slow (days) for monovalent cations.[39,40] Slow but continuous ion adsorption to the IL increases the local ionic strength, thus promoting gel formation and long-term instability.

This section ends with considerations on the nature of the lamellar phase. The typical $d_{(100)}$ from SAXS/SANS (**Figure S 3**) is broader than what is classically found in lamellar phases and could be interpreted as a nematic phase,[41] or as a coagel-to-gel transition.[42] The latter is excluded because fibrillary crystals are never observed and gel always forms below the lipid T_m. Then, if the density of defects (in PLM) is too high shown to exclude a nematic phase, other arguments support the lamellar phase: 1) WAXS experiments (**Figure S 3.b**) show the typical pattern of a lipid packing, most likely in the $P_{\beta,i}$ phase, as commented in the Supporting Information. 2) All cryo-TEM data show the systematic presence of flat sheets being "infinite" in the planar dimension, in contrast to a "finite" disk diameter in nematic phases. 3) SAXS data of glyco-hydrogels (e.g., pH 7, [NaCl]≤ 250 mM, **Figure S 3.a**) can be fitted with a lamellar form and structure factors,[43] providing a high Caillé parameter (0.9) and small number of stacked lamellae (< 10), in agreement with soft lamellar systems with short-range correlation rich in mono and divalent counterions.[38–40] Analogous SAXS profiles are also reported for biomembranes.[35] 4) The evolution of $d_{(100)}$ with ionic strength and d_{ideal} at low lipid fractions are typical of lipid lamellar phases.[34,35] 5) PLM (**Figure S 2.g-j**) shows the typical whispy defectuous texture of lamellar a phase.

Mechano-structural characterization of G-C18:0 lamellar hydrogels using *in-situ* rheo-SAXS

In view of developing soft G-C18:0 hydrogels-based materials, it is crucial to understand the effect of three independent stimuli, pH, temperature and shear rate, on the mechanical and structural properties of the gels. pH, temperature and shear respectively affect the sol-gel transition, the membrane softening and the lamellar packing. The mechano-structural characterization of G-C18:0 hydrogels is performed by combining rheo-SAXS (apparatus shown in **Figure S 6)**, cryo-TEM and optical microscopy.

Effect of pH. G-C18:0 has an apparent pKa of 8.4 ± 0.1 (**Figure S 7**) and micelle-to-lamellar transition pH of about 7.8, below which the ionization degree is estimated to < 0.2 (**Figure S 7**).[19,20] Above pH 8, the solution is fluid, while below pH 8 the viscosity increases. Increasing and decreasing pH respectively promote gel-to-sol and sol-to-gel transitions and in the following we explore the latter on the mechanical and structural properties of the gel.

Approaching the sol-to-gel transition by manual addition of HCl is a possible but tedious, uncontrolled, process due to local formation of gelly aggregates. For this reason, we employ glucono-δ-lactone (GDL)[44] to reduce pH in a more homogeneous way. GDL, which hydrolyzes into gluconic acid, is an acidifier commonly used to prepare strong low-molecular weight gels without interfering with the self-assembly process.[45] The time evolution of the viscoelastic properties during sol-gel shows a rapid increase of G´ and G´´ within the initial 10 min, generally corresponding to a sharp pH drop, before a lag time spanning between 3 and 4 hours, during which the slope G´(t) varies significantly (**Figure 3c, recorded** in a couette cell and **Figure S 8** in a plate-plate geometry). After formation of the gels (G´> G´´), and at sufficiently long lag time, the moduli are practically constant (**Figure S 8**), and G´ can reach values up to 10^4 Pa. This value is astonishingly high for a lamellar hydrogels below 10 wt%, especially if compared to the typical values of G´ at plateau found in polymer-stabilized

phospholipid and polymer-free lamellar hydrogels (G´< 10^3 Pa)[16,26,46] or in onion (5 wt%, L'_α, G´~ 10 Pa) and onion+lamellar (15 wt%, L'_α+L_α, G´~ 10^2 Pa) phases found for nonionic surfactants in water.[47] One should note that G´´> G´ at time below 250 min (**Figure 3c**) is an artifact due to the couette cell geometry, which does not impose a constant normal force, differently than the plate-plate geometry, where G´ is always higher than G´´ (**Figure S 8**). G´(ω) and G´´(ω) (**Figure 3d**) display the same dependency with the angular frequency as seen for the as-prepared hydrogels at constant pH and given ionic strength (**Figure 2b**), thus showing that the method of preparation does not affect the nature of the gel but only the plateau elastic modulus. Finally, ^{1}H NMR experiments show that the fraction of G-C18:0 in the lamellar phase is practically quantitative (95 %) and stable over time (**Figure S 9**).

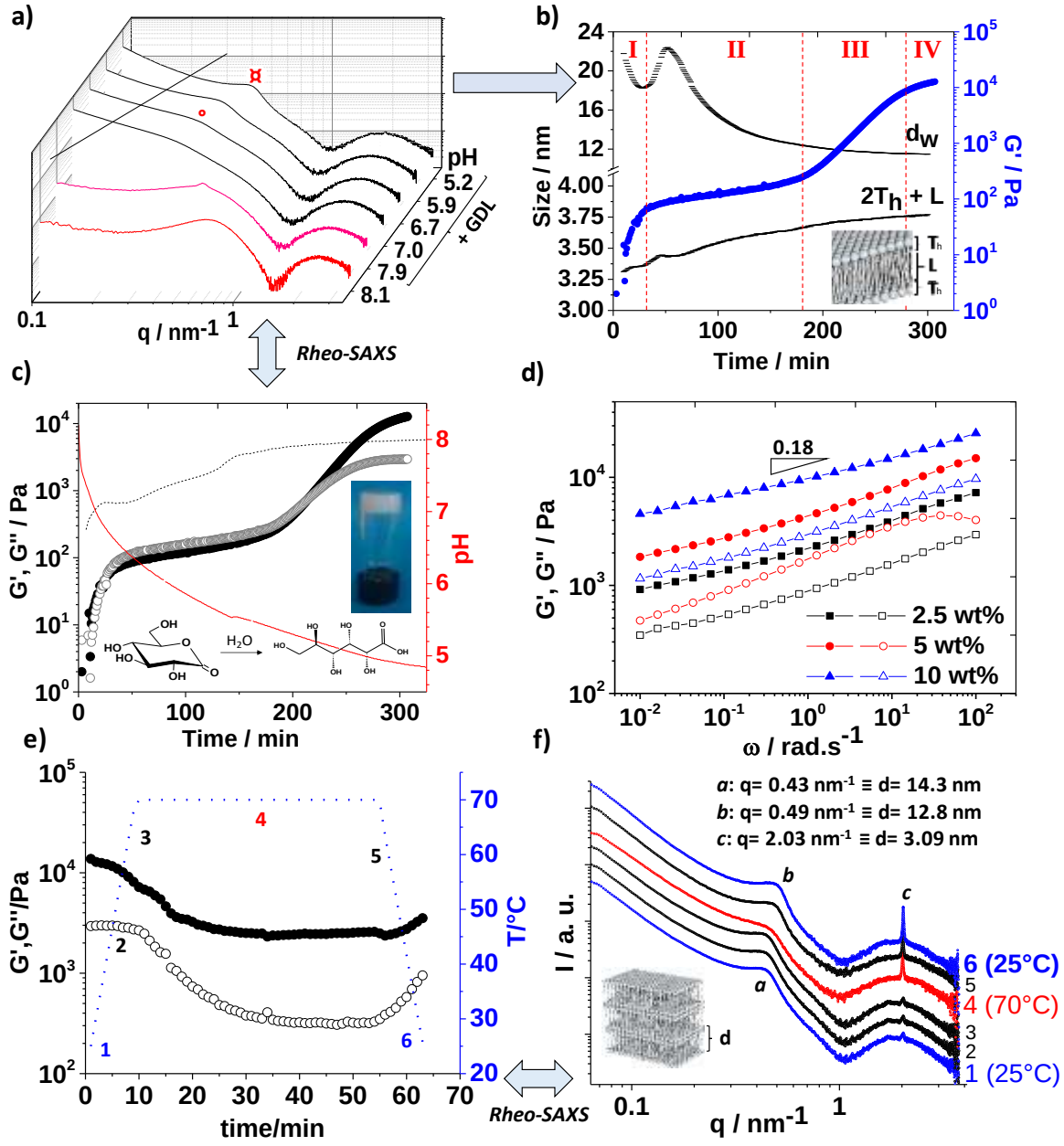

Figure 3 – a-c) GDL-driven sol-to-gel transition probed using rheo-SAXS ($C_{G\text{-}C18:0}$= 5 wt%, initial pH 8.1, [GDL]= 100 mM). a) Selected SAXS profiles of the rheo-SAXS experiment in (b). Modelling of the SAXS data is shown in Figure S 10. Symbols ° and ¤ indicate the broad peak attributed to the lamellar stacking. b) Time evolution of water layer, d_w, and IL membrane, ($2T_h$+L), thickness derived from SAXS data analysis of rheo-SAXS data in (a). Blue symbols correspond to G´ in (c). c) Time evolution of G´ (full symbols), G´´ (open symbols) (ω= 6.28 rad·s^{-1}, γ= 0.1%, constant gap 1 mm, couette cell geometry) and pH (red curve). The G´´> G´ at t> 50 min is an artifact most likely due to the constant gap of the couette cell, because no multiple cross-over exists in the cone-plate geometry with constant normal force (Figure S 8). The dotted line represents the G´ at 5 wt% presented in Figure S 8 and collected under constant normal

force. d) G´(ω) (full symbols) and G´´(ω) (open symbols) measured for 2.5 wt% < $C_{GC18:1}$ < 10 wt% measured after 720 min (γ= 0.1 %) from addition of GDL (initial pH 8.1). e) Time evolution of G´ (full symbols), G´´ (open symbols) of the same sample presented in (c) after reaching G´ at plateau at T= 25°C and upon application of a temperature ramp of 5°C/min from 25°C to 70°C. Temperature is held at 70°C for 60 min, then brought back to T= 25°C at 5°C/min (temperature profile is shown in blue). f) Selected SAXS experiments corresponding at rheology data (rheo-SAXS) presented in (e); numbers are related to the temperature profile in (e). d refers to the interlamellar distance.

Figure 3a presents representative SAXS patterns recorded during the sol-to-gel transition (**Figure 3c**) from pH 8 min to pH 5. The SAXS profiles below 15 min are typical for a micellar phase and largely characterized for the G-C18:0 in a previous work.[19] Below pH 8, the oscillation at q> 1 nm^{-1} and the broad peaks (indicated by symbols ° and ¤) at q< 1 nm^{-1} respectively characterize the lamellar form factor and d-spacing, as discussed above. The numerical fit of the SAXS data corresponding to the lamellar phase (typical fits are shown in **Figure S 10**) provides the water layer, d_w, and IL IL thickness ($2T_h$+L, respectively hydrophilic shell thickness and hydrophobic core length).

The viscoelastic properties during the sol-to-gel transition can be divided into four regions (**Figure 3b**): *I*) *t< 40 min*: sharp increase of both moduli up to 10^2 Pa, pH reaches ~6.5 and d_w decreases from 22 nm to 18 nm: region I is characterized by an increase in the concentration of lamellae per unit volume due to the completion (t ~40 min, **Figure S 9**) of the micelle-lamellar transition; *II*) *50 < t/min < 170* is characterized by a pseudo-plateau, both moduli slowly increase with time, d_w increases back to 22 nm before dropping towards 12 nm. The reasons for such an oscillating behavior of d_w are not clear, because they could depend on many coexisting factors like electrostatic repulsion due to an excess of negatively-charged glucolipids in the IL, variation in the salt concentration at the membrane but also variations in the osmotic pressure between the lamellar domains and the bulk solution; *III*)

200<t/min<300 and *IV*) *t>300 min* are respectively characterized by a sharp increase and stabilization of G´ and G´´, with d_w~12 nm: lowering of pH reduces the charge density (less COO^- groups) in the IL , resulting in closer lamellae.

In summary, rheo-SAXS shows that the sol-to-gel process is characterized by a micelle-to-lamellar transition, as found before under dilute conditions.[19] The hydrogel formation is a dynamic process passing through the assessment of the interlayer distance, dominated by d_w (rather than the IL thickness), of which the fall below ~15 nm is strongly correlated to the improvement of the mechanical properties.

Effect of temperature. Shear and fast heating above the T_m were employed in the experiments in **Figure 2** to anneal the gels and allow comparable rheology experiments. To decorrelate the combined effects of temperature and shear, we study hereafter the effect of temperature on the mechano-structural properties of a G-C18:0 gel at rest by *in-situ* rheo-SAXS.

Figure 3e quantifies the loss of the mechanical properties of a typical G-C18:0 hydrogel at rest (C= 5 wt%, G´ at plateau ~ 10^4 Pa) of about one order of magnitude between 25°C and 70°C. When temperature is decreased again to 25°C, the system recovers most of its mechanical properties after an equilibration time of 30 min to 60 min. Interestingly, temperature alone at rest, differently than pH, does not promote a gel-to-sol transition in the 25°C-70°C range, because G´ > G´´ (at ω= 6.28 rad.s^{-1}, γ= 0.1%) even at 70°C. Rheo-SAXS experiments show that the scattering profile of SAXS at 25°C is very similar to the profile at 70°C, except for the *a*-peak at q= 0.43 nm^{-1} (d-spacing, 14.3 nm) at 25°C (profile 1 in **Figure 3f**) becoming broader at 70°C (profile 4 in **Figure 3f**). Broadening indicates an increasing local disorder. Reversibility is also confirmed by the data collected after cooling at 25°C, where the peak recovers its original width (profile 6 in **Figure 3f**), although with slightly smaller d-spacing (12.8 nm). Softening of the gel characterized by the same IL structure could

be compatible features with formation of a vesicular-lamellar gels, known to have poorer mechanical properties than purely lamellar hydrogels.[12,47,48] However, differently than expected, confocal microscopy seem to exclude the formation of vesicles but rather the enhancement of spherulitic domains of few micrometers in size composed of highly curved disordered lamellar sheets (**Video 4,5**, recorded at C= 2.5 wt%, pH 6 and T= 50°C). Temperature also promotes an increased fraction of condensed lamellae, as demonstrated by the systematic and irreversible increase in the intensity of *c*-peak at 2.03 nm^{-1}. Macroscopically, it is not uncommon to observe a precipitate after heating and cooling.

In summary, temperature (in the absence of shear) promotes a reversible order-disorder transition, characterized by the presence of spherulitic disordered lamellar aggregates, which soften the G-C18:0 hydrogel. The gel can be recovered with its original elastic properties upon cooling but precipitation of a dense lamellar phase could be expected.

Effect of shear. Shear is a key processing parameter when working with gels and in the specific case of lamellar phases, two main non-equilibrium phase transitions under shear occur: shear-induced orientation[49] or multi-lamellar vesicles (onion phase).[50,51] The shear thinning flow behavior of a lamellar phase is generally explained by the gliding of the layers relative to each other due to screw dislocations, which slide under an applied shear to counterbalance the applied vorticity,[52] or by layer tilting and dilation under shear flow, which could lead to a continuous production of dislocations.[53] Rheo-SAXS and microscopy help picturing these phenomena when shear is applied to a G-C18:0 lamellar hydrogel.

The decrease of dynamic viscosity, η, with shear rate, $\dot{\gamma}$, (Figure 4a) depicts a typical shear-thinning behavior of the lamellar hydrogel. $\eta(\dot{\gamma})$ profiles, recorded on G-C18:0 hydrogels prepared in Figure 3c, display shear-thinning properties both during (t=120 min, G´~ 10^2 Pa) and after (t>300 min, G´~ 10^4 Pa) gelation but after 300 min, the zero-shear

plateau is two orders of magnitude higher and the shear thinning behavior is reversible (upon decrease in the shear rate, the system recovers its original viscosity). At t>300 min, the lamellae are isotropically oriented from zero-shear to well above 10 s^{-1}, above which a mild orientation occurs up to 1000 s^{-1}, in contrast to classical orientation under shear in lamellar systems.[49] On the contrary, below 200 min (**Figure 4a)**, lamellar orientation is more sensitive to shear: isotropic orientation at zero shear (pattern 1) is lost between 0.1 s^{-1} and 1 s^{-1} (pattern 2), where the first order Bragg reflection now clearly appears, indicating a perpendicular alignment of the lamellae with respect to the shear direction (**Figure 4b**). Between 10 s^{-1} and 100 s^{-1}, the $\eta(\dot{\gamma})$ profile is characterized by a jump (observed using plate-plate, cone-plate and couette cell geometries) and the SAXS pattern (3) shows a partial loss lamellar alignment, due to either a change in the orientation, from perpendicular to parallel, or to partial disordering. Optical differential interference contrast microscopy (DIC-M) and cryo-TEM performed on sheared G-C18:0 glyco-hydrogels show the presence of both aligned lamellae (DIC-M) and condensed structured spheroids (DIC-M and Cyo-TEM) (**Figure 4c**) and exclude the presence of an onion phase.[50,51]

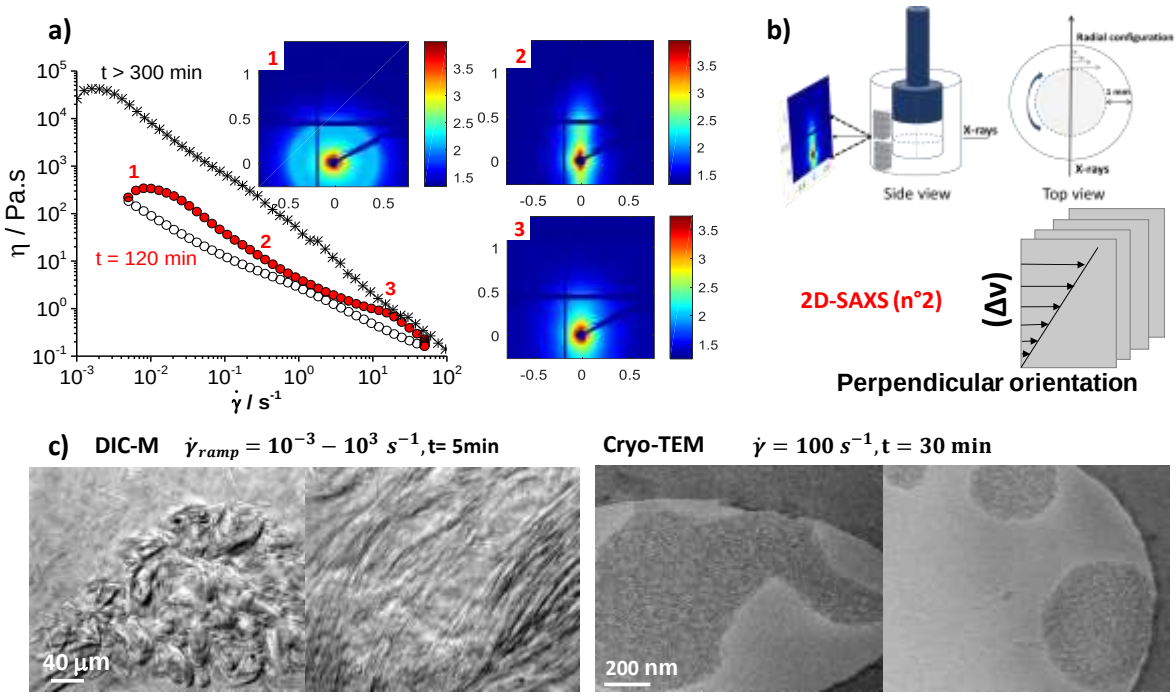

Figure 4 - a) Evolution of viscosity η with shear rate $\dot{\gamma}$ recorded on G-C18:0 hydrogel prepared in Figure 3c after 120 min (G´~ 10^2 Pa, red: ascending shear rate ramp; white: decreasing shear rate ramp) and after 300 min (G´~ 10^4 Pa, stars) at $C_{G\text{-}C18:0}$= 5 wt% (constant gap 1 mm, couette cell geometry, [GDL]= 100 mM). Images 1-3 are representative 2D SAXS patterns corresponding to 1-3 in the η($\dot{\gamma}$) profile. b) Scheme representing the rheo-SAXS geometry and the perpendicular orientation from the 2D SAXS pattern n°2. c) DIC-M and cryo-TEM images are recorded on the lamellar glyco-hydrogel (pH~6, $C_{G\text{-}C18:0}$= 5 wt% and $C_{G\text{-}C18:0}$= 1 wt%, respectively) after shear. Shearing conditions are given on top of each micrograph.

In summary, rheo-SAXS combined with microscopy show a transition from lamellar to structured spheroids, which, to the best of our knowledge, was never described in the literature on lipid IL. Such finding seems however in agreement with the predicted folding of a stiff flat system,[54] predicted theoretically in the so-called crumpling transition,[55] observed on graphene oxide sheets.[56] T_m higher than RT and the possible $P_{\beta,i}$ phase characterizing G-C18:0 hydrogels may explain the stiffness and such unexpected behaviour under shear, instead of a lamellar-to-vesicle transition, classically obtained in L_α phases.

Rheo-thinning and fast recovery are used to prepare kinetically-trapped soft anisotropic 3D materials

The kinetically-trapped state, heterogeneity, and responsivity to external stimuli of the lamellar glyco-hydrogels may seem a drawback when it comes to a precise control of the mechanical properties. However, hereafter we show that these characteristics can be exploited at one's favour. **Figure S 11** shows that a typical hydrogel (2.5 wt%, pH 6, [NaCl]= 123 mM) submitted to a series of step-strain (0.5 % < γ < 100 %) cycles is able to recover about 25% of its initial elasticity after 30 s and between 60% and 80% after 30 min. If Na^+ is replaced by divalent Ca^{2+}, we have observed a general tendency to form a stiffer hydrogel faster with a delayed 'negative' aging (from gel to precipitate) from days to weeks. The interaction of Ca^{2+} divalent cations with lipid IL is a complex,[57,58] but effective, faster,[39,40] and somewhat a different[59] phenomenon than monovalent cation adsorption. When a $CaCl_2$ solution is added to a G-C18:0 lamellar glyco-hydrogel (2.5 wt%, prepared at pH ~6.7), the gel aspect becomes denser, strongly scattering and precipitation at [$CaCl_2$]= 50 mM (**Figure 5a**). The addition of 10 mM $CaCl_2$ increases remarkably G´ and G´´ values by a decade, showing the discussed power law dependency of frequency for both moduli (**Figure 5b**). However, excess Ca^{2+} (here, 20 mM $CaCl_2$) dramatically lowers the mechanical properties, confirming the data collected at high [Na^+] (**Figure 2b**). After three cycles of step strain experiments, the G-C18:0 lamellar glyco-hydrogels at 0, 5, 10 and 20 mM $CaCl_2$ respectively recover 70 %, 77 %, 69 % and 31 % of their initial G´ values after 30 min, demonstrating their potential use in soft material engineering.

Processing of soft self-assembled materials is of a great importance and a lot of work has been devoted to fibrillary soft materials,[60] while shaping of lamellar systems is generally performed on polymeric materials,[61] because the engineering of lamellar hydrogels was not mature enough up to now. Based on the shear-thinning properties of G-C18:0 lamellar glyco-

hydrogels and the kinetic trapping effect of Ca^{2+}, we are able to prepare shape-defined soft 3D materials by either continuous (fibers) or dropwise (beads) extrusion of a 2.5 wt% G-C18:0 lamellar glyco-hydrogel into a $CaCl_2$ solution (**Figure 5d**).[62] PLM (**Figure 5**) performed on the beads and fibers confirm the expected heterogeneous, highly defectuous, lamellar structure of the Ca^{2+}-trapped gels, in analogy analogous to PLM images recorded on lamellar glyco-hydrogels with high NaCl content (**Figure 2.d** and **Figure S 2.g-h**).

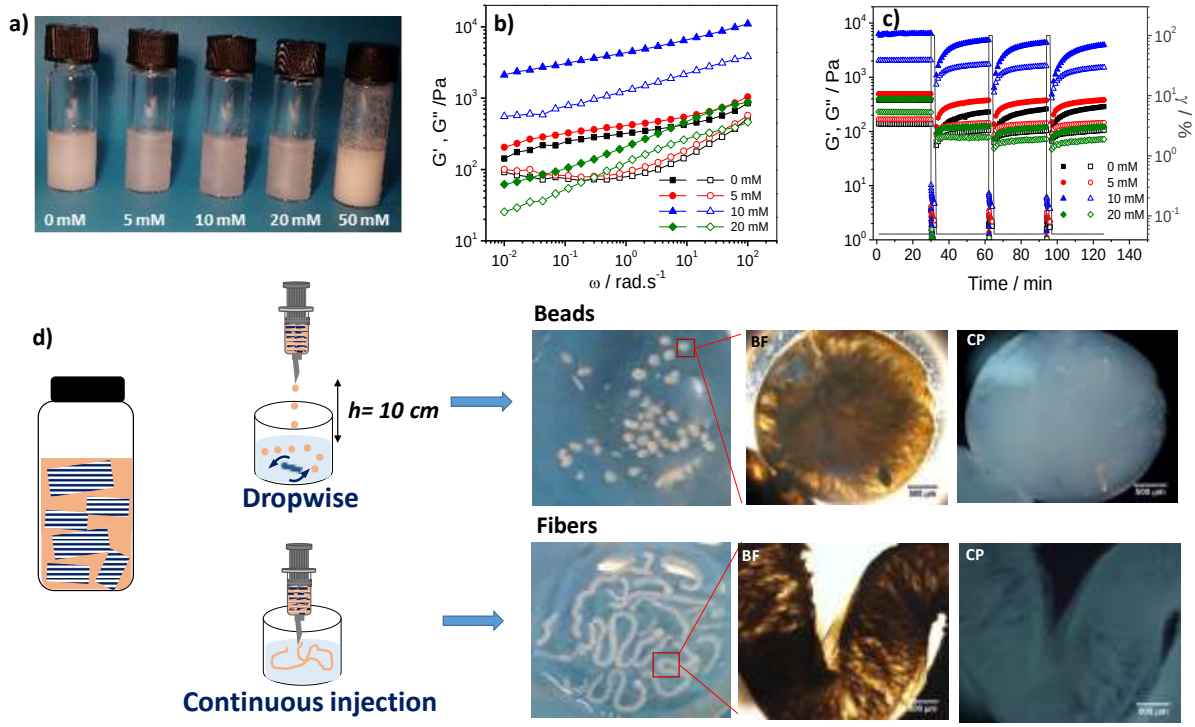

Figure 5 – a) G-C18:0 (2.5 wt%, pH ~ 6.7) lamellar glyco-hydrogels at increasing $CaCl_2$ concentration. b) G´(ω) (full symbols) and G´´(ω) (open symbols) performed on samples in a) (γ = 0.05 %, lag time 2 h). c) Three cycles of step-strain experiments (ω= 6.28 $rad{\cdot}s^{-1}$, destructuring at γ=100 % during 2 min followed by recovery at γ= 0.05 % during 30min) performed on samples in a). G´ is represented by full symbols. d) Soft G-C18:0 lamellar glyco-hydrogel materials obtained by extruding a rheo-thinning hydrogel in a $CaCl_2$ (1 M) solution. PLM microscopy (Brigth Field, BF, and Crossed Polarizers, CP) images show the biphasic and defectuous nature of the kinetically-trapped hydrogels.

In summary, we show that a new pH-responsive glucolipid obtained in large amounts from glucose and vegetable oils from the microbial fermentation of the modified yeast *S. bombicola ΔugtB1* is able to form lamellar rheo-thinning glyco-hydrogels in water in the pH range between 5 and 7.5 and ionic strength between 10 mM and 500 mM. Hydrogels are composed of a biphasic medium composed of water and large interconnected domains (100-500 μm) of kinetically-trapped lamellar phase controlled by electrostatic interactions. The mechanical properties depend on both the high density of defects, as expected, but also on the multiscale structure where lamellar domains of several hundred microns coexist with domains of few microns and disordered spherulitic inclusions composed of entangled lamellar sheets of thickness less than 500 nm. pH and shear enhance sol-gel transitions, ionic strength below ~500 mM consolidates the hydrogel, while temperature at rest weakens the mechanical properties through order-disorder transitions. Interestingly, homogeneous pH variations can promote gels with elastic moduli as high as $G' \sim 10^4$ Pa. We exploit the sensitivity to pH and ionic strength to prepared 3D soft lamellar materials by a simple extrusion process in a Ca^{2+} solution. This work shows the huge potential of new biobased compounds, the key to a future biobased economy, having functional, stimuli-responsive, properties that outclass the best standards in the field. Considering the biocompatibility of the glucolipid and large production potential, we expect novel applications in medicine, tissue engineering and, at the same time, the astonishing mechanical properties of the lamellar glyco-hydrogels should stimulate research in the field of complex fluids and biophysics, including 3D printing.

Acknowledgements: Experimental and technical assistance: Dr. Andrea Lassenberger (SANS, ILL, Grenoble, France), Mr. Abdoul Aziz Ba (Sorbonne Université, Paris, France), Mrs Chloé Seyrig (Sorbonne Université, Paris, France), Dr. Patrick Davidson (PLM, LPS, Université Paris Sud, Orsay, France), Prof. Gijsje Koenderink and Mrs. Federica Burla (Rheo-

SAXS, AMOLF Institute, Amsterdam, Netherlands), Dr. Francisco Fernandes (Sorbonne Univerité, Paris, France). Helpful discussions (lamellar phase and hydrogels, rheology, Rheo-SAXS): Dr. Jack Leng (LOF-CNRS, Bordeaux, France), Prof. Ulf Olsson (University of Lund, Lund, Sweden), Dr. Patricia Bassereau (Institut Curie, France), Frédéric Nallet (University of Bordeaux, Bordeaux, France), Dr. Bruno Demé (ILL, Grenoble, France), Dr. Thibaut Divoux (Massachusetts Institute of Technology, Cambrigde, MA, USA), Dr. Lionel Porcar (ILL, Grenoble, France).

Funding: European Community's Seventh Framework Programme (FP7/2007–2013) under Grant Agreement No. Biosurfing/289219; European Synchrotron Radiation Facility (ESRF), Grenoble, France, under the experiment number SC 4778; Institut Laue Langevin (ILL), Grenoble, France, under the experiment number 9-13-778; SasView application, originally developed under NSF award DMR-0520547 and funding from the European Union's Horizon 2020 (SINE2020 project, grant agreement No 654000).

Author contributions: GBM and NB performed the hydrogel experiments, analyzed the data and wrote the manuscript. PG performed cryo-TEM experiments. SP provided assistance on the SANS experiments. DHM set-up the rheo-SAXS experiments. WS and SR synthesized the glucolipid. CVS performed the hydrogenation experiments of the glucolipid.

Competing Interests: All authors declare no conflicts of interests.

Supplementary Materials:

Materials and Methods

Figs. S1 to S11

Supplementary text

Video 1 through Video 5 can be downloaded at https://mycore.core-cloud.net/index.php/s/bV3BV8Bn0dpNh11

References:

1 G. M. Whitesides and B. A. Grzybowski, *Science (80-.).*, 2002, **295**, 2418–2421.

2 L. A. Haines, K. Rajagopal, B. Ozbas, D. A. Salick, D. J. Pochan and J. P. Schneider, *J. Am. Chem. Soc.*, 2005, **127**, 17025–17029.

3 M. R. Dreher, A. J. Simnick, K. Fischer, R. J. Smith, A. Patel, M. Schmidt and A. Chilkoti, *J. Am. Chem. Soc.*, 2008, **130**, 687–694.

4 S. Toledano, R. J. Williams, V. Jayawarna and R. V. Ulijn, *J. Am. Chem. Soc.*, 2006, **128**, 1070–1071.

5 X. Zhuang, Y. Mai, D. Wu, F. Zhang and X. Feng, *Adv. Mater.*, 2015, **27**, 403–427.

6 T. E. Wilkop, J. Sanborn, A. E. Oliver, J. M. Hanson and A. N. Parikh, *J. Am. Chem. Soc.*, 2014, **136**, 60–63.

7 M. L. Mather and P. E. Tomlins, *Regen. Med.*, 2010, **5**, 809–821.

8 A. Ainla, I. Gözen, B. Hakonen and A. Jesorka, *Sci. Rep.*, 2013, **3**, 2743.

9 M. J. Webber, E. A. Appel, E. W. Meijer and R. Langer, *Nat. Mater.*, 2015, 15, 13–26.

10 J. Israelachvili, *Intermolecular and Surface Forces*, 2011.

11 M. A. Haque, G. Kamita, T. Kurokawa, K. Tsujii and J. P. Gong, *Adv. Mater.*, 2010, **22**, 5110–5114.

12 H. E. Warriner, S. H. Idziak, N. L. Slack, P. Davidson and C. R. Safinya, *Science (80-.).*, 1996, **271**, 969–73.

13 M. Ilyas, M. A. Haque, Y. Yue, T. Kurokawa, T. Nakajima, T. Nonoyama and J. P. Gong, *Macromolecules*, 2017, **50**, 8169–8177.

14 K. Steck, J. H. van Esch, D. K. Smith and C. Stubenrauch, *Soft Matter*, 2019.

15 S. Koitani, S. Dieterich, N. Preisig, K. Aramaki and C. Stubenrauch, *Langmuir*, 2017.

16 J. Niu, D. Wang, H. Qin, X. Xiong, P. Tan, Y. Li, R. Liu, X. Lu, J. Wu, T. Zhang, W. Ni and J. Jin, *Nat. Commun.*, 2014, **5**, 3313.

17 C. Y. Cheng, T. Y. Wang and S. H. Tung, *Langmuir*, 2015, **31**, 13312–13320.

18 C. Stubenrauch and F. Gießelmann, *Angew. Chemie - Int. Ed.*, 2016, **55**, 3268–3275.

19 N. Baccile, A. S. Cuvier, S. Prévost, C. V. Stevens, E. Delbeke, J. Berton, W. Soetaert, I. N. A. Van Bogaert and S. Roelants, *Langmuir*, 2016, **32**, 10881–10894.

20 N. Baccile, M. Selmane, P. Le Griel, S. Prévost, J. Perez, C. V Stevens, E. Delbeke, S. Zibek, M. Guenther, W. Soetaert, I. N. A. Van Bogaert and S. Roelants, *Langmuir*, 2016, **32**, 6343–6359.

21 K. M. J. Saerens, J. Zhang, L. Saey, I. N. A. Van Bogaert and W. Soetaert, *Yeast*, 2011, **28**, 279–292.

22 O. Palme, G. Comanescu, I. Stoineva, S. Radel, E. Benes, D. Develter, V. Wray and S. Lang, *Eur. J. Lipid Sci. Technol.*, 2010, **112**, 663–673.

23 A. Brakemeier, D. Wullbrandt and S. Lang, *Biotechnol. Lett.*, 1998, **20**, 215–218.

24 N. Baccile, L. Van Renterghem, P. Le Griel, G. Ducouret, M. Brennich, V. Cristiglio, S. L. K. W. Roelants and W. Soetaert, *Soft Matter*, 2018, **14**, 7859–7872.

25 G. Ben Messaoud, P. Le Griel, D. Hermida-Merino, S. L. K. W. Roelants, W. Soetaert, C. V. Stevens and N. Baccile, *Chem. Mater.*, 2019, DOI: 10.1021/acs.chemmater.9b01230.

26 H. E. Warriner, P. Davidson, N. L. Slack, M. Schellhorn, P. Eiselt, S. H. J. Idziak, H. W. Schmidt and C. R. Safinya, *J. Chem. Phys.*, 1997, **107**, 3707–3722.

27 J. C. Stendahl, M. S. Rao, M. O. Guler and S. I. Stupp, *Adv. Funct. Mater.*, 2006, **16**, 499–508.

28 A. Jaishankar and G. H. McKinley, *Proc. R. Soc. A Math. Phys. Eng. Sci.*, 2013, **469**.

29 F. Gobeaux, E. Belamie, G. Mosser, P. Davidson and S. Asnacios, *Soft Matter*, 2010, **6**, 3769–3777.

30 H. H. Winter and F. Chambon, *J. Rheol. (N. Y. N. Y).*, 1986, **30**, 367.

31 P. Sollich, F. Lequeux, P. Hébraud and M. E. Cates, *Phys. Rev. Lett.*, 1997, **78**, 2020–2023.

32 P. Sollich, *Phys. Rev. E - Stat. Physics, Plasmas, Fluids, Relat. Interdiscip. Top.*, 1998, **58**, 738–759.

33 H. J. Hwang, R. A. Riggleman and J. C. Crocker, *Nat. Mater.*, 2016, **15**, 1031–1036.

34 T. Dvir, L. Fink, R. Asor, Y. Schilt, A. Steinar and U. Raviv, *Soft Matter*, 2013, **9**, 10640–10649.

35 A. Steiner, P. Szekely, O. Szekely, T. Dvir, R. Asor, N. Yuval-Naeh, N. Keren, E. Kesselman, D. Danino, R. Resh, A. Ginsburg, V. Guralnik, E. Feldblum, C. Tamburu, M. Peres and U. Raviv, *Langmuir*, 2012, **28**, 2604–2613.

36 H. E. Warriner, S. L. Keller, S. H. J. Idziak, N. L. Slack, P. Davidson, J. A. Zasadzinski and C. R. Safinya, *Biophys. J.*, 1998, **75**, 272–293.

37 M. M. A. E. Claessens, B. F. Van Oort, F. A. M. Leermakers, F. A. Hoekstra and M. A. C. Stuart, *Biophys. J.*, 2004, **87**, 3882–3893.

38 G. Brotons, M. Dubois, L. Belloni, I. Grillo, T. Narayanan and T. Zemb, *J. Chem. Phys.*, 2005, **123**.

39 O. Szekely, A. Steiner, P. Szekely, E. Amit, R. Asor, C. Tamburu and U. Raviv, *Langmuir*, 2011, **27**, 7419–7438.

40 O. Lotan, L. Fink, A. Shemesh, C. Tamburu and U. Raviv, *J. Phys. Chem. A*, 2016, **120**, 3390–3396.

41 P. Davidson, C. Penisson, D. Constantin and J.-C. P. Gabriel, *Proc. Natl. Acad. Sci.*, 2018, **115**, 6662–6667.

42 E. Carretti, V. Mazzini, E. Fratini, M. Ambrosi, L. Dei, P. Baglioni and P. Lo Nostro, *Phys. Chem. Chem. Phys.*, 2016, **18**, 8865–8873.

43 F. Nallet, R. Laversanne and D. Roux, *J. Phys. II*, 1993, **3**, 487–502.

44 Y. Pocker and E. Green, *J. Am. Chem. Soc.*, 1973, **95**, 113–119.

45 D. J. Adams, M. F. Butler, W. J. Frith, M. Kirkland, L. Mullen and P. Sanderson, *Soft Matter*, 2009, **5**, 1856–1862.

46 P. Versluis, J. C. Van de Pas and J. Mellema, *Langmuir*, 2001, **17**, 4825–4835.

47 O. Regev and F. Guillemet, *Langmuir*, 1999, 4357–4364.

48 M. Gradzielski, *J. Phys. Condens. Matter*, 2003, **15**, R655.

49 C. R. Safinya, E. B. Sirota, R. F. Bruinsma, C. Jeppesen, R. J. Piano and L. J. Wenzel, *Science (80-.).*, 1993, **261**, 588–591.

50 O. Diat, D. Roux and F. Nallet, *J. Phys. II Fr.*, 1993, **3**, 1427–1452.

51 A. G. Zilman and R. Granek, *Eur. Phys. J. B*, 1999, **11**, 593–608.

52 C. Meyer, S. Asnacios and M. Kléman, *Eur. Phys. J. E*, 2001, **6**, 245–253.

53 C. Y. D. Lu, P. Chen, Y. Ishii, S. Komura and T. Kato, *Eur. Phys. J. E*, 2008, **25**, 91–101.

54 R. Lipowsky, *Handb. Biol. Phys.*, 1995, **1**, 521–602.

55 P. Le Doussal and L. Radzihovsky, *Ann. Phys. (N. Y).*, 2018, **392**, 340–410.

56 X. Ma, M. R. Zachariah and C. D. Zangmeister, *Nano Lett.*, 2012, **12**, 486–489.

57 A. Melcrová, S. Pokorna, S. Pullanchery, M. Kohagen, P. Jurkiewicz, M. Hof, P. Jungwirth, P. S. Cremer and L. Cwiklik, *Sci. Rep.*, 2016, **6**, 38035.

58 O. Shih, Y. Q. Yeh, K. F. Liao, C. J. Su, P. H. Wu, R. K. Heenan, T. Y. Yu and U. S. Jeng, *J. Phys. Chem. Lett.*, 2018, **9**, 4287–4293.

59 M. Javanainen, A. Melcrová, A. Magarkar, P. Jurkiewicz, M. Hof, P. Jungwirth and H. Martinez-Seara, *Chem. Commun.*, 2017, **53**, 5380–5383.

60 S. Zhang, M. A. Greenfield, A. Mata, L. C. Palmer, R. Bitton, J. R. Mantei, C. Aparicio, M. O. De La Cruz and S. I. Stupp, *Nat. Mater.*, 2010, **9**, 594–601.

61 Y. F. Yue, M. A. Haque, T. Kurokawa, T. Nakajima and J. P. Gong, *Adv. Mater.*, 2013,

25, 3106–3110.

62 D. L. Gin, W. Gu, B. A. Pindzola and W. J. Zhou, *Acc. Chem. Res.*, 2001, **34**, 973–980.

Supplementary Information for

Single-Lipid Lamellar Hydrogels: from Gel Engineering to Soft Materials Design

Ghazi Ben Messaoud, Patrick Le Griel, Sylvain Prévost, Daniel Hermida-Merino, Wim Soetaert, Sophie L. K. W. Roelants, Christian V. Stevens, Niki Baccile*

Correspondence to: niki.baccile@sorbonne-universite.fr

This PDF file includes:

Materials and Methods

Figs. S1 to S11

Supplementary text

References for SI reference citations

Video 1 through Video 5 are downloadable at

https://mycore.core-cloud.net/index.php/s/bV3BV8Bn0dpNh11

Supplementary Information Text

Materials and Methods

Chemicals. The microbial monunstaurated glucolipid G-C18:1 has been produced at a production rate of ~ 0.5 $gL^{-1}h^{-1}$ in a bioreactor system using a modified strain (*ΔugtB1*) of the yeast *Starmerella bombicola*[1] and according to the experimental conditions described in ref. [2]. The fully saturated G-C18:0 (M_w = 462.6 $g.mol^{-1}$), used in this work, was obtained from GC18:1 by a catalytic hydrogenation reaction, described in ref. [2]. The NMR, HPLC and LC-MS analyses of G-C18:0 can be found in ref. [2]. Glucono-δ-lactone (GDL, M_w = 178.14 $g.mol^{-1}$) was purchased from Sigma Aldrich. 18:1 Liss Rhod PE (M_w= 1301.7 $g.mol^{-1}$, λ_{abs}= 560 nm, λ_{em}= 583 nm), 1,2-dioleoyl-sn-glycero-3-phosphoethanolamine-N-(lissamine rhodamine B sulfonyl) (ammonium salt), is purchased by Avanti® Polar, Inc

General method to prepare G-C18:0 hydrogels. Hydrogels are prepared by dispersing the G-C18:0 sample in water followed by sonication and adjustment of pH to the desired pH value and ionic strength. In detail, a given amount of G-C18:0 (in wt%) is dispersed in a given volume of milliQ water (generally 1 mL). The pH of the mixture is generally between 3.5 and 4.5, according to the sample concentration. The pH is then adjusted in the range 5.5 - 7.5 using 1-20 µL of NaOH 1 M (0.1 M can also be used for refinement), according to concentration and desired pH. The mixture is then sonicated between 15 and 20 min in a classical sonicating bath to reduce the size of the aggregated powder and until obtaining a homogenous, viscous, dispersion. To this solution, the desired volume of NaCl is added so to obtain a given total $[Na^+]$ {= [NaOH] + [NaCl]} molar concentration. To keep the dilution factor negligible, we have used a 5 M concentrated solution of NaCl. The mixture is then sonicated again during 15 min to 20 min and eventually vortexed two or three times during 15 s each. The solution can then be left at rest during 15 min to 30 min. This procedure is generally enough to obtain a stable hydrogel. However, to reduce the impact of gel history, measurements done in Figure 2 and Figure S 3 have been performed after 2 hours following an annealing cycle: vortexing of the gel during 15 s at room temperature, loading of the fluid solution in the rheometer, heating from 25°C to 70°C (above T_m) at 10°C/min, rest at T= 70°C during 10 min, cooling to T= 25°C at 10°C/min.

Other methods to prepare G-C18:0 hydrogels. The method given above, although by far the easiest most efficient and reproducible approach, is not unique in preparing G-C18:0

hydrogels, of which the synthesis is highly versatile. Below, we provide other equivalent methods, which were developed to be adapted to specific analytical or experimental conditions. The two crucial parameters are the final pH and total ion concentration, and it seems that the process through which these parameters are fixed is not important. However, the process may influence the homogeneity of the solution and to this regard it is not excluded that the absolute value of the elastic modus at plateau may depend on the process.

- *Sample preparation method for rheo-SAXS experiments (Figure 3 and Figure 4 in the main text). In-situ* rheo-SAXS analysis is a powerful technique to probe the mechano-structural properties of the hydrogels and it was used here to study, among other, the sol-to-gel transition which occurs between basic and acidic pH. For this set of experiments, we have developed a complementary method to prepare the hydrogel. A given amount of G-C18:0 (in wt%) is first dispersed in 1 mL of water and sonicated for few minutes to break the aggregated powder. The pH of the solution is then raised under stirring with few µL (generally between 2 and 30, according to the amount of sample) of 5 M NaOH until pH ~9-10 is reached. The solution becomes a partially clear sol at basic pH, (pH > 8) as discussed in a previous work.[2] The sol-to-gel transition is then studied using an *in situ* acidification using glucono δ-lactone (GDL). A given amount of GDL is weighted in a vial, to which the basic G-C18:0 solution is added. Mixing is achieved by vortexing for approximately 10 to 20 seconds and the sample is allowed to stand still (no additional vortexing, sonication, stirring) with gelation taking place over several hours at room temperature. For the rheo-SAXS experiments, the G-C18:0 solution at basic pH is immediately placed in the couette cell after mixing with GDL. A constant GDL: G-C18:0 molar ratio of 1.08:1 is selected. Indeed, to prepare G-C18:0 solutions of 10, 25, 50 and 100 $mg.mL^{-1}$, concentrations of GDL of 3.56, 8.9, 17.8 and 35.6 $mg.mL^{-1}$ were selected, respectively.
- *Sample preparation method to develop soft materials (Figure 5 in the main text).* A rheo-thinning G-C18:0 hydrogel ($C_{G\text{-}C18:0}$= 2.5 wt%, pH~6.7, V= 10 mL) is first prepared by pH-jump method using HCl. The hydrogel is then divided in five vials (V= 1.9 mL per each) and different volumes of $CaCl_2$ solution ([CaCl2]=1 M) are added. The final volumes are then adjusted to 2 mL using Milli-Q-grade water and the mixtures are vortexed during 30 sec to achieve a complete homogenization. The final $CaCl_2$ concentrations are (0, 5, 10, 20 and 50 mM).

Small Angle X-ray Scattering (SAXS). All SAXS experiments are performed at 25°C at the DUBBLE BM26B beamline at the ESRF synchrotron facility (Grenoble, France).[3,4] Dialyzed samples (please refer to the preparation of the hydrogel section) have been analysed during the run SC4639 using a beam at 11.93 KeV and a sample-to-detector distance of 2.10 m. Samples are prepared ex-situ and they are analysed directly by setting them in front of the x-ray beam. The signal of the Pilatus 1M 2D detector (172 x 172 μm pixel size), used to record the data, is integrated azimuthally with PyFAI to obtain the *I(q) vs. q* spectrum ($q = 4\pi \sin\theta/\lambda$, where 2θ is the scattering angle) after masking systematically wrong pixels and the beam stop shadow. Silver behenate ($d_{(100)}$ = 58.38 Å) and α-Al_2O_3 ($d_{(012)}$ = 3.48 Å) are respectively used as SAXS and WAXS standards to calibrate the q-scale. Data are not scaled to absolute intensity.

Rheo-SAXS. Experiments coupling rheology and SAXS have been performed during the SC4778 run using a beam energy of 12.65 KeV and a sample-to-detector distance of 3.23 m, where silver behenate is used as q-calibration standard. A MCR 501 rheometer (Anton Paar, Graz, Austria) equipped with a Couette polycarbonate cell (gap 1 mm) was coupled to the beamline and controlled through an external computer in the experimental hutch using the Rheoplus/32 V3.62 software. A radial scattering configuration, where the beam passes the sample along the velocity gradient direction, was used. The rheology and SAXS acquisitions are synchronized manually with an estimated time error of less than 5 s. Due to standard security procedures, the first rheo-SAXS experimental point is systematically acquired with a delay of about 3-4 minutes. The experimental setup is shown on **Figure S 6**. SAXS signal acquisition and processing is the same as above. Data are not scaled to absolute intensity.

Small Angle Neutron Scattering (SANS). SANS experiments have been performed at the D11 beamline of Institut Laue Langevin (Grenoble, France). Four q-ranges have been explored and merged using the following wavelengths, λ, and sample-to-detector (StD) distances. 1) ultra-low q: λ= 13.5Å, StD= 39 m; 2) low-q: λ= 5.3Å, StD= 39 m; 3) mid-q: λ= 5.3Å, StD= 8 m; 4) high-q: λ= 5.3Å, StD= 1.4 m. All samples are prepared in 99.9% D_2O (using NaOD and DCl solutions, as well) to limit the incoherent background scattering. Solutions are analyzed in standard 1 mm quartz cells. Direct beam, empty cell, H_2O are recorded and boron carbide (B4C) is used as neutron absorber. All samples are thermalized at 70°C during 10 min then cooled down at 25°C. Analysis is performed after 2 h from cooling. The background sample

(D_2O) signal was subtracted from the experimental data. Absolute values of the scattering intensity are obtained from the direct determination of the number of neutrons in the incident beam and the detector cell solid angle. The 2-D raw data were corrected for the ambient background and empty cell scattering and normalized to yield an absolute scale (cross section per unit volume) by the neutron flux on the samples. The data were then circularly averaged to yield the 1-D intensity distribution, I(q). The software package Grasp (developed at ILL and available free of charge) is used to integrate the data, while the software package SAXSUtilities (developed at ESRF and available free of charge) is used to merge the data acquired at all configurations and subtract the background.

Analysis of the SAXS data. The lamellar phase formed by the G-C18:0 glucolipid has been previously characterized by SAXS and it was described by two symmetrical hydrophilic regions, containing the glucose and COOH moieties, separated by an interdigitated layer of the C18 chain.[2] The corresponding structural parameters are: thickness of the hydrophilic region: T_h= 1.4 nm; length of the hydrophobic core: L= 0.8 nm. The total thickness of the bilayer is then ($2T_h$+L)= 3.6 nm, where the error coming from the fitting procedure of the corresponding SAXS data is estimated to about 10%. Unless otherwise stated, we use these values to characterize the lamellae.

The rheo-SAXS experiments performed in this work have been analysed in a similar way: we combined a core-shell bicelle form factor model,[a] as in ref. [2], with a Lorentzian peak,[b] to account for the presence of the broad low-q interaction peak. We used the SasView 3.1.2 software. For the core shell bicelle form factor, we use a large value of the bicelle radius (R= 100 nm), thus mimicking a large flat object, analogous to a lamella. The rim radius is set to zero. The solvent Scattering Length Densities (SLD) are adjusted as in ref. [2]: the SLD value of H_20 is $9.4 \cdot 10^{-4}$ nm^{-1} while the core SLD is set to $8.3 \cdot 10^{-4}$ nm^{-1}, which represents a typical value for an aliphatic chain. The SLD of the hydrophilic region is set $10.9 \cdot 10^{-4}$ $Å^{-1}$. Due to the fact that we do not employ an absolute scale, the SLD values cannot be quantitatively exploited. Finally, T_h, L and the scaling factor (the latter is varied because our data are not in absolute scale) are the only variables. The Lorentzian peak is controlled by the full width at half maximum and the peak position, which are qualitatively estimated at the beginning of the fit and allowed to vary for refinement.

a http://www.sasview.org/docs/user/models/core_shell_bicelle.html

b http://www.sasview.org/docs/user/models/peak_lorentz.html

Selected data (**Figure S 3.a**) were also fitted using a core-shell lamellar form factor, *in toto* equal to the previous approach, combined with the structure factor described by Nallet *et al*.[5] for a lyotropic lamellar phase, where the lamellae are assumed to be randomly distributed in solution.[c] If the structural parameters of the lamellae (shell thickness and core length) are not affected by this approach and fit quality is the same as the one presented in **Figure S 10**, this model has the advantage to correlate, through the Caillé parameter η and the number of lamellar plates, N, the structure (amplitude, width, position) of the peak describing the interlamellar distance to the elastic properties of the lamellar phase:

$$\eta = \frac{q_0^2 k_b T}{8\pi\sqrt{K\bar{B}}} \qquad \text{Eq. 2}$$

where q_0 is the peak position, k_b is the Boltzmann constant, T is the temperature, K is the bilayer bending rigidity, $\bar{B}$ the bulk compression modulus. The Caillé parameter η is a measure for the bilayer fluctuations via the analysis of the Bragg diffraction peak of the lamellar phase. From a qualitative point of view, large values of η characterize soft membranes, while small values of η are encountered in stiff membranes.[6] Upon use of this model, η, N, thickness and length of, respectively, the hydrophilic and hydrophobic regions, are the variable parameters, while the SLD's are adjusted as described above.

Rheology. Rheology experiments are carried out using a MCR 302 rheometer (Anton Paar, Graz, Austria) equipped with a Peltier temperature system which allows accurate control of the temperature by the stainless steel lower plate and with a solvent trap to ensure minimal evaporation of water during the measurements.

- *Oscillatory rheology*. These experiments are performed using titanium or a stainless steel sandblasted upper plate (diameter 25 mm). The gap (0.5 or 1 mm) and the normal force (NF= 0 N) are controlled during the experiments. After loading, samples are allowed to stand at rest for at least two hours before analysis. A dynamic strain sweep is first conducted at an angular frequency (ω= 6.28 rad·s^{-1}) by varying the shear strain (γ) from 0.001 to 100 % in order to determine the linear viscoelastic regime (LVER). A value of strain within the LVER is then applied in the following dynamic angular frequency sweep between 100 and 0.01 rad.s^{-1}. Frequency time sweep experiments are also performed to monitor the gelation kinetic of the G-C18:0 samples by slow acidification. Briefly, the glucolipid basic solution is mixed with the appropriate amount of GDL and the final mixture is vortexed for 20 seconds and immediately

c http://www.sasview.org/sasview/user/models/model_functions.html#lamellarpshgmodel

loaded on the bottom plate. Dynamic oscillatory time sweep experiments are then performed by applying a constant angular frequency (ω = 6.28 rad·s^{-1}) and a shear strain (γ) within the LVER (0.05 - 0.1 %) and data are collected during 720 minutes at 25 °C. A delay of 3-5 minutes occurs between the moment of mixing and the beginning of the measurement. To monitor the gelation of the G-C18:0 upon thermal annealing, the elastic (G´) and viscous (G´´) moduli are recorded during temperature heating ramps from 20 to 70 °C at a rate of 10 °C/min. The sample is initially vortexed, then loaded and held at 70 °C for 10 min and then cooled from 70 to 25 °C at a rate of 10 °C/min and finally held at 25°C during two hours. These temperature variation experiments are performed using an oscillation angular frequency (ω= 6.28 rad·s^{-1}) and a strain (γ = 0.05%). Afterward, an angular frequency sweep (100 – 0.01 rad·s^{-1}) was performed using a shear strain, γ= 0.05%, within the LVER.

- *Shear viscosity*. Steady-shear viscosity is determined using a cone-and-plate geometry (diameter 25 mm, angle 1° and truncation 50 µm) and a plate-and-plate geometry (diameter 25 mm, gap = 0.5 mm) by increasing the shear rate (γ) from 10^{-3} to 10^{3} s^{-1}. Compared to plate-plate geometry, cone-plate configuration guarantee a uniform shear of the sample, however the small imposed gap (truncation 50 µm) could lead to preferential aggregation of the lamellar structure (3-4 nm of thickness but few µm of length ($L_{lamellar}$) in the center of the geometry ($L_{lamellar}$ > gap x 10). Here we presented therefore the data obtained used the plate-plate geometry. Except for thermal annealing experiments, all rheological characterizations are conducted at 25 °C, unless otherwise mentioned.

Sample imaging.

Light Microscopy. Images of G-C18:0 samples, at rest or after shear, are acquired in bright field and polarized light mode (PLM) using a Nikon DS-Ri1 through crossed polarizers and in a differential interference contrast mode (DIC-M) using a Zeiss AxioImager D1 microscope.

Cryogenic Transmission Electron Microscopy (Cryo-TEM). These experiments were carried out on an FEI Tecnai 120 twin microscope operating at 120 kV equipped with a Gatan Orius CCD numeric camera. The sample holder was a Gatan Cryoholder (Gatan 626DH, Gatan). On both microscopes, Digital Micrograph software was used for image acquisition. Cryofixation was done on a homemade cryofixation device. The solutions were deposited on

a glow-discharged holey carbon coated TEM copper grid (Quantifoil R2/2, Germany). Excess solution was removed and the grid was immediately plunged into liquid ethane at −180 °C before transferring them into liquid nitrogen. All grids were kept at liquid nitrogen temperature throughout all experimentation.

Nuclear Magnetic Resonance (NMR): time-resolved ^{1}H solution NMR experiments are acquired on a Bruker Avance III 300 spectrometer using a 5 mm ^{1}H-X BBFO probe. Number of transient is 16 with 5 s recycling delay. Experiments are carried out as follows: a 5 wt% solution prepared in D_2O (500 µL) at pD ~11 is mixed with 100 mM GDL at RT, inserted in a standard 5 mm NMR tube and immediately introduced in the NMR spectrometer. The entire process before requires about 6 min from the moment of mixing to first acquired ^{1}H NMR scan. Absolute values of the peak area as a function of time are obtained using the *integration* and *relaxation* moduli of the Topspin™ 3.5 pl7 version of the software. We have observed that phasing problems due to change in pH may affect the peak of residual H_2O. Since this is the most intense peak, poor phasing can affect the baseline in the vicinity of the sugar C<u>H</u> region between 3 ppm and 4.5 ppm. This unavoidable fact strongly affects the actual value of the peak area. For this reason, we mainly present the time-resolved evolution of the aliphatic peak area, contained between 0.8 ppm and 3 ppm. Peak area normalization is performed with respect to the spectrum recorded before adding GDL, when the entire G-C18:0 population is detected in the micellar phase. The integrated signal corresponds to the molar fraction of G-C18:0 in the soluble micellar phase, defined X_M. The fraction of G-C18:0 in the lamellar phase, X_L, is simply obtained by $1-X_M$, according to the assumption that the mobility in the lamellar environment is so slow that becomes "invisible" to solution NMR. This hypothesis is commonly verified in many self-assembled hydrogels.[7,8]

Differential Scanning Calorimetry (DSC): DSC is performed using a DSC Q20 apparatus from TA Instruments equipped with the Advantage for Q Series Version acquisition software (v5.4.0). Acquisition is performed on a G-C18:0 dry powder sample (~ 10 mg) sealed in a classical aluminium cup and using an immediate sequence of heating (from 10°C to 90°C) and cooling (from 90°C to 10°C) ramps both at a rate of 1°C/min.

Confocal Laser Scanning Microscopy (CLSM): CLSM was performed with a LeicaSP8 Tandem Confocal system. Samples were excited with the dye specific wavelength (561 nm) and the emission was detected between 580 and 620 nm using a photomultiplier tube (PMT) detector. CLSM images were analyzed using Fiji (Fiji is just ImageJ)[9] and 3D construction

was performed using the 3D Stack mode of Fiji. Temperature variation (T= 50°C) was performed with temperature controller modulus of the microscope. The hydrogel ($C_{G\text{-}C18:0}$= 2.5 wt%, pH 6) was prepared following the general method described above. A volume of 4 µL of an ethanolic solution of 18:1 Liss Rhod PE (C= 53 mg/mL) was added to 1.5 mL of the hydrogel to reach an approximate molar ratio of G-C18:0/Liss of 500. Liss is a water insoluble, rhodamine-containing, lipid and it is largely used to mark lipid bilayers. It is generally considered not to interfere with the bilayer assembly at Lipid/Liss ratio above 200. We did not observe any variation in the gel physical aspect after addition of Liss.

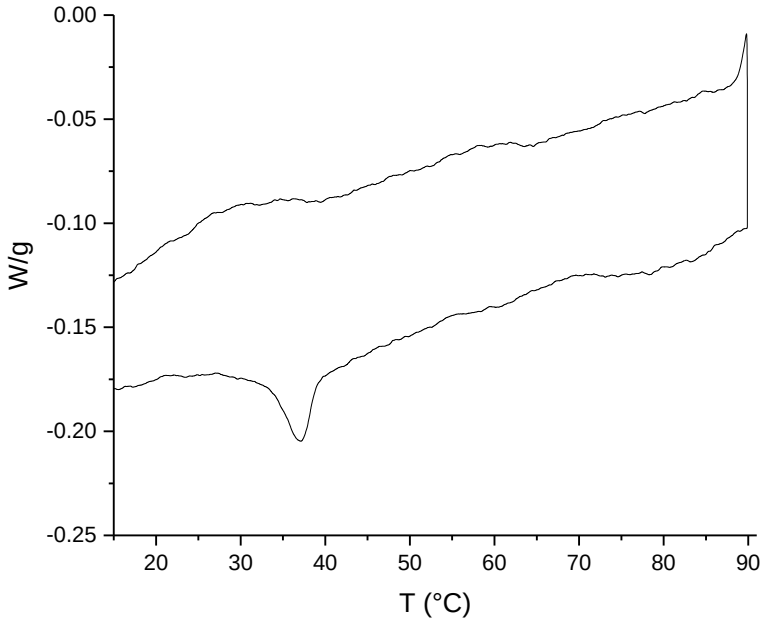

Figure S 1 – Differential Scanning Calorimetry (DSC) thermogram of the native G-C18:0 powder acquired at 1°C/min

1 wt%, pH 6.5, liquid

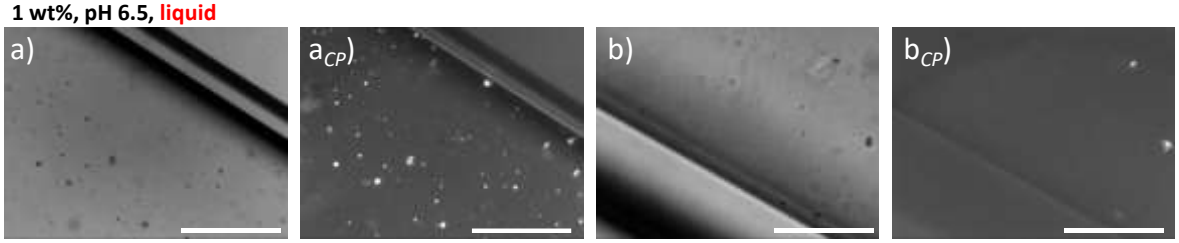

2.5 wt%, pH 6.5, 30 mM NaCl, viscous

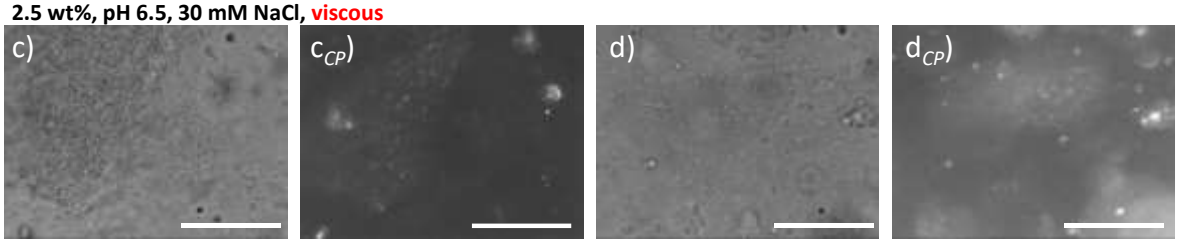

2.5 wt%, pH 6.5, T=60°C, 30 mM NaCl, liquid

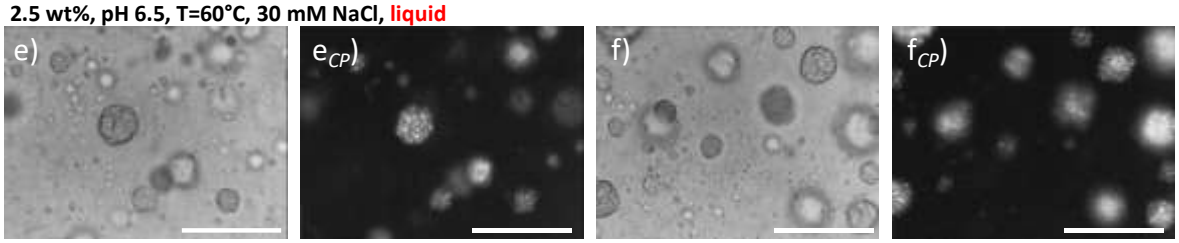

2.5 wt%, pH 6.5, 150 mM NaCl, gel

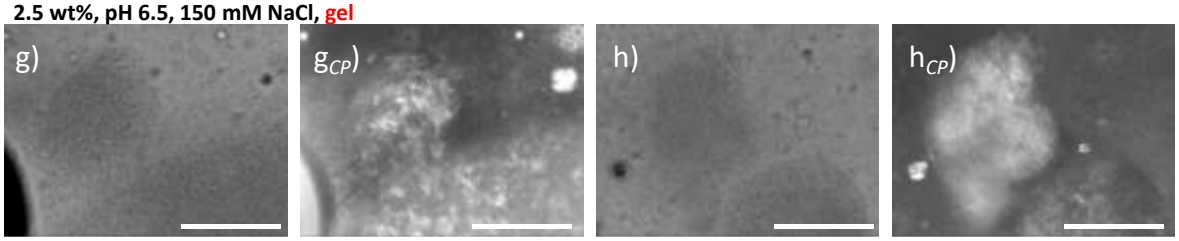

Highlight: 2.5 wt%, pH 6.5, 150 mM NaCl, gel

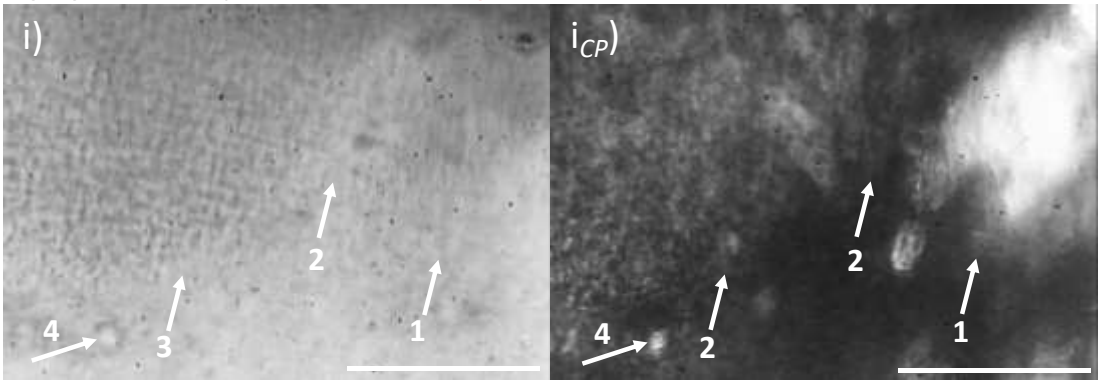

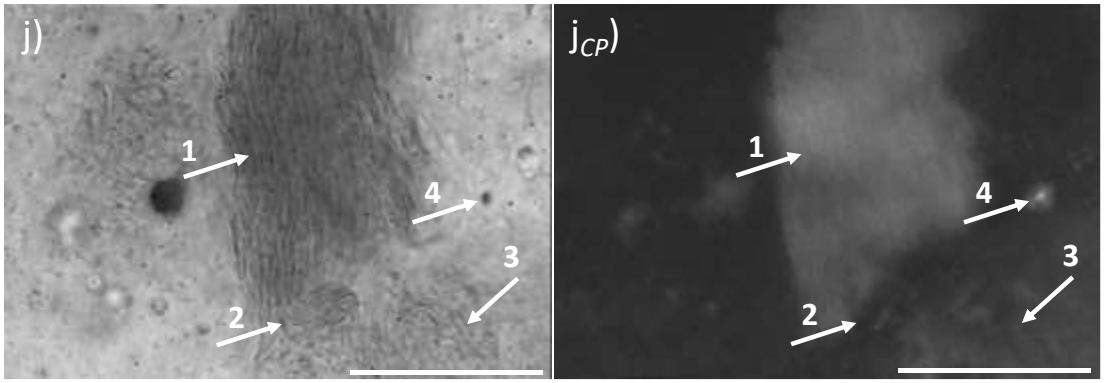

Figure S 2 – Bright Field and PLM (scale bar: 100 μm) of a set of G-C18:0 samples at pH 6.5 in water. Samples are prepared in flame-sealed flat capillary of 200 μm thickness, as in ref. [10]. Exact conditions are given on top of each series of images. All images are recorded after 24 h from preparation. All samples are kept at room temperature ~ 23°C, except in images e)-f), in which samples are kept at T= 60°C. The subscript *CP* refers to the corresponding image on the immediate left acquired using crossed polarizers. The physical state of the sample are explained in red for each series of images. Images in c)-d) and e)-f) refer to the same sample, although in e)-f) the sample has been placed at T= 60°C. Images in i) and j) highlight the gel sample. Arrows 1 through 3 correspond to anisotropic regions with different orientations and arrow 4 to spherulitic domains.

PLM is commonly used as a complementary technique to XRD to distinguish the typical defect textures in lamellar phases, lamellar gels, nematic phases and coagels.[10–13] Unfortunately, PLM is mostly reliable when the density of defects is small and they can be isolated. **Figure S 2** presents a broad series of bright field and PLM (indicated with the *CP* subscript) image recorded on typical fluid, viscous and gel samples composed of G-C18:0 at pH 6.5. At a first glance it is possible to exclude the presence of coagels (lack of typical fibrilar crystals)[13] and, most likely, of a defectless lamellar phase (absence of oily streaks).[10] In detail, liquid samples are generally characterized by small strongly birefringent circular domains of approximate size of 1-10 μm at 1 wt% and room temperature (**Figure S 2a-b**) and 10-50 μm at 2.5 wt% (30 mM NaCl) at T= 60°C (**Figure S 2e-f**). These inclusions recall the spherulites in ref. [10] and they are dispersed in a non-birefringent medium. Nevertheless, the nature of these domains is most likely not the same; temperature is known to induce a lamellar-to-vesicle transition in this compound[2] and the 10-50 μm spherulitic domains in the sample at T= 60°C (2.5 wt%, 30 mM NaCl, **Figure S 2e-f**) correspond to vesicular compartments, probably multilamellar, given their strong birefringency.

Upon increase in viscosity (2.5 wt%, 30 mM NaCl, RT, **Figure S 2c-d**) and up to gel formation (2.5 wt%, 150 mM NaCl, RT, **Figure S 2g-h**), the medium becomes more and more characterized by larger irregular birefringent domains of whispy texture (typical size of 100-500 μm) coexisting with strongly birefringent spherulitic inclusions of smaller size (1-50 μm). Even if the high density of defects makes a clear-cut attribution risky, we must nonetheless note that such description recalls the fluid-gel transition line in lamellar gels than a nematic phase.[10] However, the lamellar gels were characterized by a monophasic lamellar domain, while **Figure S 2i-j** clearly puts in evidence the strong heterogeneity of the G-C18:0 gels. 1-labeled arrows show oriented defectuous lamellar domains similar to the whispy textures both in bright field and PLM. These domains are connected to defectuous

birefringent, although disordered, domains (arrows N° 3) through a continuous change in orientation (arrows N° 2). Finally, 4-labelled arrows point at spurious small (< 10 μm) spherulitic domains. The entire set of PLM experiments show that the G-C18:0 lamellar glyco-hydrogel is not composed of a simple defectuous single lamellar phase, as found in ref. [10], but rather composed of large (hundreds of microns) interconnected defectuous lamellar domains dispersed in water.

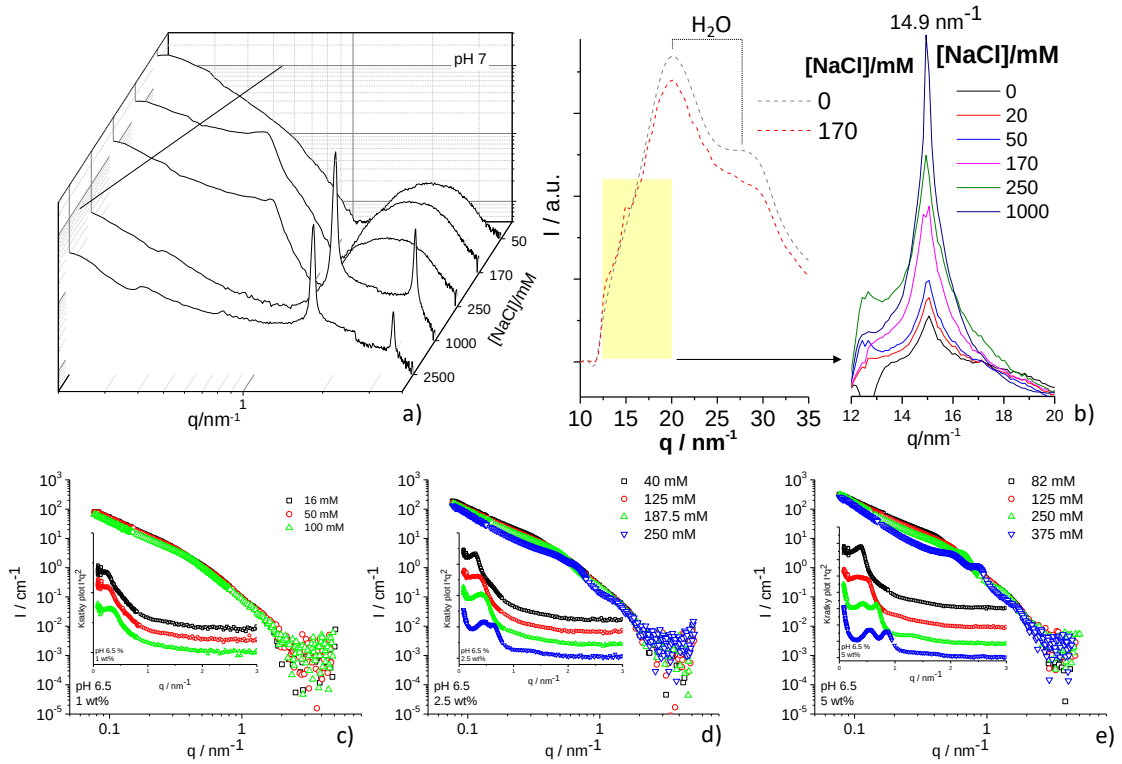

Figure S 3 – a) SAXS profiles acquired for a G-C18:0 solution (5 wt%) at pH 7 at various NaCl concentrations; b) background (water)-containing (left-hand side) and background-subtracted (right-hand side) WAXS profiles of samples studied in a); c-d) SANS profiles acquired on samples prepared at pH 6.5 and various NaCl concentrations at (c) 1 wt%, (d) 2.5 wt%, (e) 5 wt%. Insets: Kratky plots [I·q^2(q)]

Attribution of the lipid mesophase type of lamellar phase is done using the WAXS portion of the x-ray scattering data (Figure S 3b). The WAXS data show a sharp peak at 14.9 nm^{-1}: in the absence of salt, the peak is so broad that it can hardly be detected, unless background (water, characterized by the classical peaks at 20 and 27 nm^{-1}) is subtracted. Above [NaCl]= 1 M, the peak is intense and sharp. All experiments are performed at room temperature, below the T_m, thus suggesting an ordered packing of the lipids within the bilayers. It is then expected that G-C18:0 forms a $L_{\beta,i}$ phase (interdigitation comes from the bolaform nature of G-C18:0). A classical L_β is commonly characterized by an intense, well-defined, peak between 14.9 nm^{-1} and 15 nm^{-1} (d-spacing of 4.2 nm),[14–16] signature of the parallel packing of the acyl chain within the hydrophobic region of the bilayer. The collapsed phase is certainly in the form of $L_{\beta,i}$. On the contrary, in the swollen region, the same peak is very broad; according to the water-containing profiles (b), the shoulder at 14.9 nm^{-1} should be attributed to a L_α phase, characterized by a liquid-like order of the acyl chain. However, the

expected q_0 should rather be at 14.7 nm^{-1} (d-spacing of 0.46 nm),[14–16] a smaller value than what we do observe experimentally. The last possibility, probably the most plausible, is represented by the P_β phase, which is characterized by a single peak with a corresponding d-spacing around 4.2 nm and a width larger than the L_β phase (although not as large as in the L_α).[14,16]

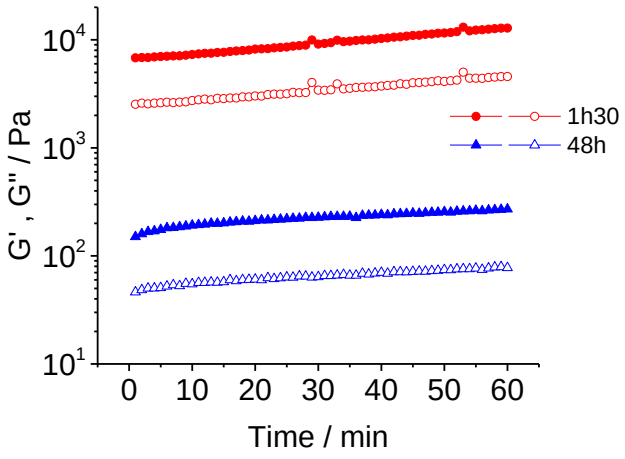

Figure S 4 – Time evolution of G' (full symbols) and G'' (open symbols) (ω= 6.28 rad.s^{-1} and γ= 0.05 %) for G-C18:0 ($C_{G\text{-}C18:0}$ = 5 wt%, pH= 6.7, [NaCl]= 167 mM) after 1h30 and 48 h from thermal annealing. Plate-plate geometry (25 mm), imposed normal force (NF = 0 N) and initial gap (0.5 mm).

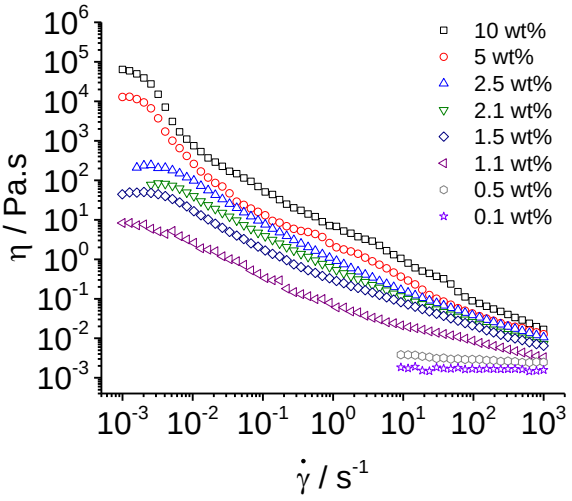

Figure S 5 – Shear thinning profiles showing the evolution of viscosity with shear rate at different G-C18:0 concentrations at pH= 6.7 ± 0.1 and [NaCl]= 163 mM. Plate-plate geometry (25 mm) and an imposed gap of 0.5 mm are used

Figure S 6 – Rheo-SAXS apparatus used at the BM29B beamline at ESRF synchrotron (Grenoble, France). A MCR 501 rheometer (Anton Paar, Graz, Austria) equipped with a Couette polycarbonate cell (imposed gap = 1 mm) is employed. A radial configuration is used during the Rheo-SAXS study.

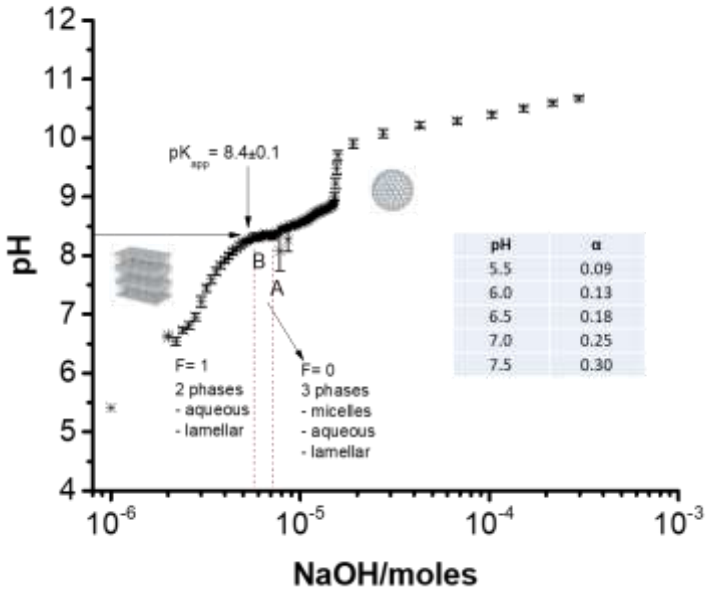

Figure S 7 – Experimental determination of the apparent pKa of glucolipid G-C18:0 by titration using NaOH in water at T= 25°C (titrated volume: 1.8 mL). The ionization degrees are estimated using the Gibb's free energy rule applied to lamellar phases composed of fatty acids[17]

Estimating the ionization degree, α, for fatty acids as a function of pH is a long-date challenge which faces the problem of liquid-solid transition and coexistence of multiple phases. The problem of calculating α is in fact the problem of estimating the pKa. For stearic acid (which composes the fatty backbone of G-C18:0), the molecular pKa measured in organic solvents is between 4.9 and 5,[18] but this value varies between 5 and 7.6 when stearic acid is contained in a micellar environment in water.[19] In this work, we use the method of Cistola et al.[17], who applied the Gibb's phase rule to the titration curve of selected fatty acids below and above the melting temperature of the aliphatic chain. The advantage of this approach is multiple: 1) it is simple; 2) it has been used on the micelle-to-lamellar phase transitions of fatty acids in water; 3) it can be applied on our own experimental data (the titration curve) on a similar system. For the detailed description of the method, one can refer to ref. [17]. In this work, the region between points A and B in Figure S 7 satisfies the condition of invariance (F= 0), where composition is fixed, while the region below B (pH= 8.3) is characterized by one degree of freedom (F= 1), where composition of the lamellar phase can vary. α is estimated between pH 5 and pH 8.3, where α= 0.5 at B.

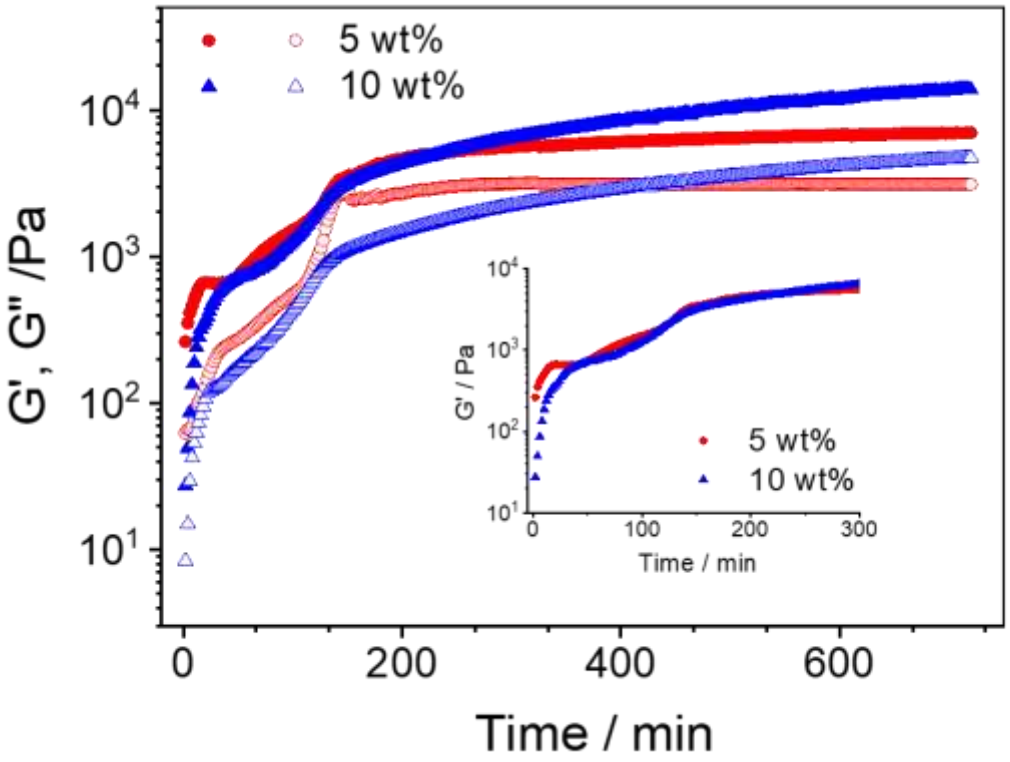

Figure S 8 – Sol-to-gel transition promoted by pH (use of GDL) through time-resolved G´ (full symbols) G´´ (open symbols) as a function of G-C18:0 concentration (initial pH 11, ω= 6.28 rad·s^{-1}, γ = 0.1%, Normal Force = 0 N, initial gap 1 mm), plate-plate geometry (25 mm), [GDL]= 100 mM at $C_{G\text{-}C18:0}$= 5 and 10 wt%)

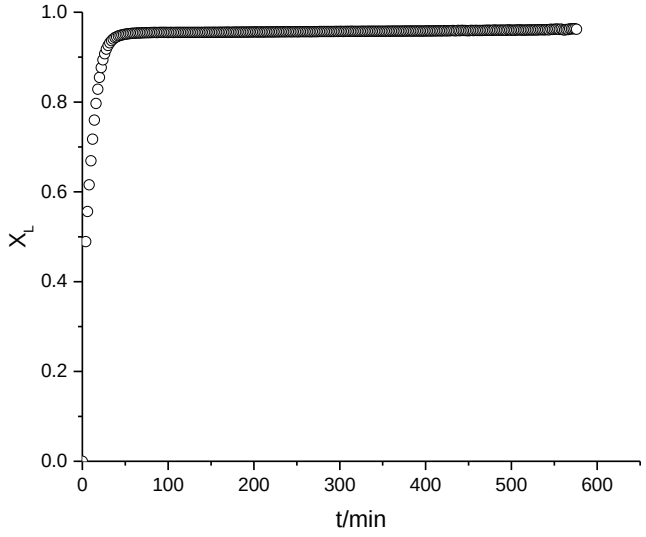

Figure S 9 – Time evolution of the molar fraction of G-C18:0 glucolipid ($C_{G\text{-}C18:0}$= 5 wt%) in the lamellar phase upon acidification (initial pH 11, [GDL]= 100 mM, solvent: D_2O). X_L= 1-X_M, where X_M, the micellar fraction, is obtained by the normalized integral of the ^{1}H NMR signal of G-C18:0 in the interval 3 < δ/ppm < 0.8. ^{1}H NMR is only sensitive to the compound in the micellar environment.

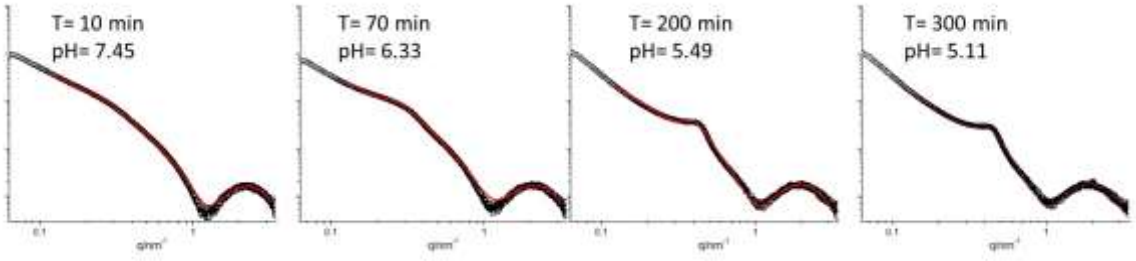

Figure S 10 – Typical fits of selected SAXS profiles acquired during the GDL hydrolysis in a G-C18:0 (5 wt%, initial pH 8.1) solution (Figure 3a in the main text). The fitting strategy has been described in the Materials and Methods section of the paper.

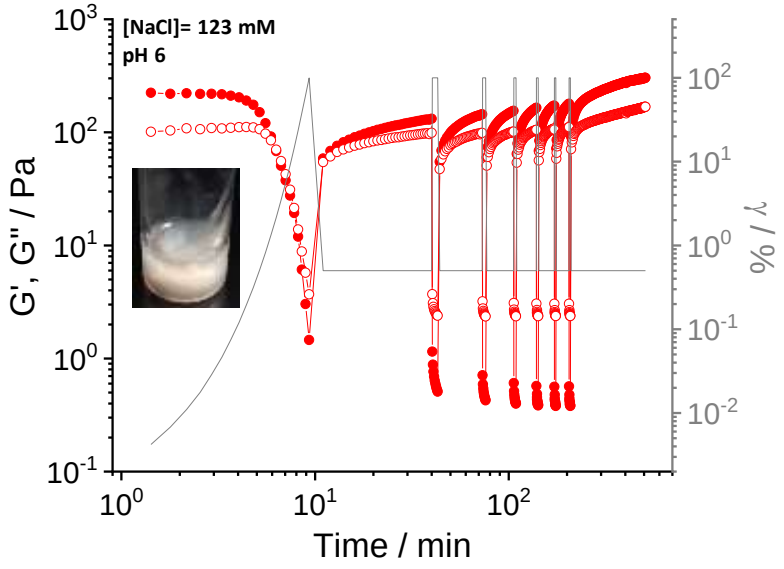

Figure S 11 – Time evolution of G' (full symbols) and G'' (empty symbols) with the imposed shear strain (γ) at angular frequency (ω= 6.28 rad·s^{-1}). Logarithmic increase of the shear strain (4·10^{-3} < γ < 100 %) during 10 min followed by a recovery at γ = 0.5 % (upper limit of the LVER) during 30 min, followed by 6 cycles of step strain experiments (γ = 100% during 2 min followed by γ = 0.5 % during 30 min (during the first 5 cycles) and 300 min in the last cycle. Plate-plate geometry (25 mm) and an imposed normal force (NF = 0 N) with an initial gap (0.5 mm) are used.

References

1 K. M. J. Saerens, J. Zhang, L. Saey, I. N. A. Van Bogaert and W. Soetaert, *Yeast*, 2011, **28**, 279–292.

2 N. Baccile, M. Selmane, P. Le Griel, S. Prévost, J. Perez, C. V Stevens, E. Delbeke, S. Zibek, M. Guenther, W. Soetaert, I. N. A. Van Bogaert and S. Roelants, *Langmuir*, 2016, **32**, 6343–6359.

3 G. Portale, D. Cavallo, G. C. Alfonso, D. Hermida-Merino, M. van Drongelen, L. Balzano, G. W. M. Peters, J. G. P. Goossens and W. Bras, *J. Appl. Crystallogr.*, 2013, **46**, 1681–1689.

4 W. Bras, I. P. Dolbnya, D. Detollenaere, R. van Tol, M. Malfois, G. N. Greaves, A. J. Ryan and E. Heeley, *J. Appl. Crystallogr.*, 2003, **36**, 791–794.

5 F. Nallet, R. Laversanne and D. Roux, *J. Phys. II*, 1993, **3**, 487–502.

6 G. Brotons, M. Dubois, L. Belloni, I. Grillo, T. Narayanan and T. Zemb, *J. Chem. Phys.*, , DOI:10.1063/1.1950667.

7 J. H. Fuhrhop, S. Svenson, C. Boettcher, E. Rössler and H. M. Vieth, *J. Am. Chem. Soc.*, 1990, **112**, 4307–4312.

8 D. J. Adams, M. F. Butler, W. J. Frith, M. Kirkland, L. Mullen and P. Sanderson, *Soft Matter*, 2009, **5**, 1856–1862.

9 J. Schindelin, I. Arganda-Carreras, E. Frise, V. Kaynig, M. Longair, T. Pietzsch, S. Preibisch, C. Rueden, S. Saalfeld, B. Schmid, J.-Y. Tinevez, D. J. White, V. Hartenstein, K. Eliceiri, P. Tomancak and A. Cardona, *Nat. Methods*, , DOI:10.1038/nmeth.2019.

10 H. E. Warriner, P. Davidson, N. L. Slack, M. Schellhorn, P. Eiselt, S. H. J. Idziak, H. W. Schmidt and C. R. Safinya, *J. Chem. Phys.*, 1997, **107**, 3707–3722.

11 S. L. Keller, H. E. Warriner, C. R. Safinya and J. A. Zasadzinski, *Phys. Rev. Lett.*, 1997, **78**, 4781–4784.

12 H. E. Warriner, S. L. Keller, S. H. J. Idziak, N. L. Slack, P. Davidson, J. A. Zasadzinski and C. R. Safinya, *Biophys. J.*, 1998, **75**, 272–293.

13 E. Carretti, V. Mazzini, E. Fratini, M. Ambrosi, L. Dei, P. Baglioni and P. Lo Nostro, *Phys. Chem. Chem. Phys.*, 2016, **18**, 8865–8873.

14 B. A. Cunningham, A. D. Brown, D. H. Wolfe, W. P. Williams and A. Brain, *Phys. Rev. E - Stat. Physics, Plasmas, Fluids, Relat. Interdiscip. Top.*, 1998, **58**, 3662–3672.

15 M. Nadler, A. Steiner, T. Dvir, O. Szekely, P. Szekely, A. Ginsburg, R. Asor, R. Resh, C. Tamburu, M. Peres and U. Raviv, *Soft Matter*, 2011, **7**, 1512.

16 A. Tardieu, V. Luzzati and F. C. Reman, *J. Mol. Biol.*, 1973, **75**, 711–733.

17 D. P. Cistola, J. A. Hamilton, D. Jackson and D. M. Small, *Biochemistry*, 1988, **27**, 1881–1888.

18 J. R. White, *J. Am. Chem. Soc.*, 1950, **72**, 1859–1860.

19 M. Ptak, M. Egret-Charlier, A. Sanson and O. Bouloussa, *Biochim. Biophys. Acta - Biomembr.*,

1980, **600**, 387–397.